International Journal of Dynamics and Control (2025) 13:106
https://doi.org/10.1007/s40435-025-01604-x

Improving a reaction curve-based analytical identification technique for fractional models

Juan J. Gude[1] · **Pablo García Bringas**[2]

Received: 24 December 2024 / Revised: 26 January 2025 / Accepted: 27 January 2025

Abstract

A new analytical procedure for identifying fractional first-order plus dead-time (FFOPDT) models has recently been proposed. The technique is applicable to systems with S-shaped step responses and involves selecting three specific points on the process response curve for parameter estimation. In a simplified version of the method, the points are symmetrically positioned as $x_1 = x\%$, $x_2 = 50\%$, and $x_3 = (100 - x)\%$, with $0 < x < 50\%$, requiring only the optimal position of one point, x, given that the others are set automatically. This study explores the effect of adjusting the value of x_2 in the representative points (x-x_2-$(100-x)\%$), while preserving symmetry around the center of the interval. Simulations provide insights into the influence of x_2 for more accurate estimation, revealing that the accuracy of the identified FFOPDT model is highly sensitive to the position of x_2, and an optimal value is proposed to enhance precision. Experimental validation on a thermal-based prototype deployed on a microprocessor confirms the technique's applicability. This approach provides new insights into selecting the central point x_2 and its implications for industrial applications.

Keywords Fractional models · Fractional systems · Identification method · Process identification

1 Introduction

For a long time, there has been a recognized need to represent a wide variety of real dynamic processes by means of reduced-order integer models. The technical literature offers a vast selection of identification techniques, with those on the basis of open-loop step experiments being among the most popular [1, 2].

Among these open-loop techniques, methods focusing on adjusting various points of the reaction curve using first-order plus dead-time (FOPDT), dual-pole plus dead-time (DPPDT) and second-order plus dead-time (SOPDT) models are particularly noteworthy. This approach is both popular and widely adopted in the process industry due to its straightforward and simple application [3]. When examining two- and three-point techniques, references [4–6] can be categorized in the first group, while methods in [7–9] fall under the second group. The technique outlined in [4] bridges both groups depending on the model employed: it is classified as a two-point technique when applied to FOPDT or DPPDT models and as a three-point technique when applied to the SOPDT model.

Additionally, the aforementioned integer-order model identification techniques can be divided according to the symmetry of the points relative to $x_2 = 50\%$. For the two-point approaches mentioned, the set is asymmetrical, with the exception of the 123c identification technique proposed in [4], which is symmetrical. Regarding the three-point approaches, references [7, 9] use asymmetrical sets, whereas reference [4] considering SOPDT models and reference [8] present symmetrical sets, although the central point used in the last method is not $x_2 = 50\%$.

In the past few decades, the advent of advanced computational methods for fractional-order calculus has provided additional evidence that specific dynamical processes can be more accurately characterized considering models of non-integer order. For example, studies such as [10, 11] present some results in the area of fractional-order modeling of real-world phenomena, while [12, 13] suggest that

✉ Juan J. Gude
jgude@deusto.es

Pablo García Bringas
pablo.garcia.bringas@deusto.es

[1] Department of Computing, Electronics and Communication Technologies, Faculty of Engineering, University of Deusto, Avda. de las Universidades, 24, 48007 Bilbao, Bizkaia, Spain

[2] Department of Mechanics, Design and Industrial Management, Faculty of Engineering, University of Deusto, Avda. de las Universidades, 24, 48007 Bilbao, Bizkaia, Spain

Published online: 22 February 2025

fractional-order models can describe thermal conduction processes with higher accuracy. In fact, fractional calculus has proven essential for both the scientific and industrial communities [14, 15], offering a valuable and powerful tool for numerous real-world applications, particularly in modeling [16]. The successful application of fractional-order models has enhanced interest in this area. Significant advances in the identification of these models have been reported in the state of the art. For example, [17] reports the first concurrent determination of model coefficients and differentiation orders through nonlinear programming. Various methods for estimating reduced-order fractional models from process reaction curves are well-documented in academic and industrial studies, with nonlinear optimization being the most commonly adopted approach in industry [18–20].

The identification of fractional-order systems with delay is examined in [21]. Similarly, [22, 23] investigate the application of non-ideal step inputs for identifying integer-order systems. Building on these ideas, [24] proposes an innovative method for identifying fractional-order systems employing non-ideal step inputs.

The above methods typically minimize the discrepancy observed between the step response of the process and the one for the approximate model of non-integer order. Note that these techniques demand a higher computational effort in comparison with some other analytical techniques.

Nevertheless, the technical literature does not offer many analytical techniques that stand out for their simplicity of application. The following papers present an analytical approach. Various techniques for determining FFOPDT model parameters employing process reaction curve data are explored in the literature. Reference [25] is considered a pioneering work in FFOPDT model parameter estimation. It outlines three distinct approaches for determining the parameters of the approximate non-integer model. A similar approach with integral-based estimation methods, which are robust against measurement noise, is proposed in [26, 27]. The latter two methods can be treated as extensions of the already available integral approaches for the classical case [3].

Given the importance of fractional-order models to accurately represent real-world phenomena, and the availability of numerous controller tuning methods based on simple process models [28–31], it is essential to obtain a reduced-order fractional model for a process. This need is one of the primary motivations of this paper.

The popularity of these methods is generally due to three reasons: First, identification algorithms based on two- or three-point fitting on the response curve are easily both understood and applied, second, understanding the physical interpretation of the response of such a process to a step signal is simple, and finally, these algorithms are straightforward to implement on hardware devices. Therefore, the extension of this type of methods to the fractional-order case can be considered a natural progression. To this end, a comprehensive identification technique has been recently introduced and detailed in [32]. The proposed approach can be considered as a generalization of the classical three-point identification procedure considering fractional-order models. This procedure is identical to the classical case. It consists of collecting process data that results from applying an open-loop step experiment, while considering a three-point set (x_1-x_2-x_3%) of the response curve. In the same framework, the approach addressed in [33] can be treated as a simplification of the preceding general technique, since the selected points are symmetrically situated with respect to the middle of the output interval. Since the selected points are x%, 50%, and $(100-x)$%, only the optimal selection of x, with $0 < x < 50$, is required. The procedure outlined in [34] utilizes the asymptotic behavior of the Mittag-Leffler function to improve the accuracy of fractional-order estimation, while the remaining model parameters are estimated using analytical expressions.

Although the symmetrical identification method proposed in [33] has been shown to yield favorable results compared to other identification procedures, this paper aims to demonstrate the sensitivity of the fractional model to variations in the location of x_2, showing that adjusting this location can further improve model accuracy while preserving the extreme points symmetrically positioned. Furthermore, the applicability and effectiveness of the symmetrical identification procedure with arbitrary x_2 will be verified when implemented on a hardware platform based on microprocessor and applied to an experimental temperature-based laboratory equipment.

The key contributions of the proposed method, compared to existing techniques, are as follows:

1. Sensitivity to x_2 position: The study reveals that the accuracy of the identified FFOPDT model is significantly sensitive to the position of x_2.
2. Impact analysis of x_2: An insight has been gained into the impact of moving x_2 on the accuracy of the identified model.
3. Central point selection: The optimal position of x_2 has been studied, demonstrating that selecting $x_2 = 65\%$ significantly improves the precision of the approximate fractional model.
4. Simulation validation: The effectiveness and performance of the proposed FFOPDT model identification technique has been evaluated by simulating several process models with different fractional-order dynamics, ensuring its broad versatility.
5. Experimental validation: The practical applicability of the technique has been verified through its implementation on a microprocessor-based experimental prototype, validating its performance in real-world scenarios.

The structure of this document is the following. Section 2 introduces the theoretical framework necessary for the development of this study. Section 3 outlines the general procedure for estimating the FFOPDT model using a set of three points of the process response. Section 4 defines the issue and outlines the approach used to address it. In Sect. 5, simulation results are presented, demonstrating that adjusting the position of x_2 within the set (x-x_2-$(100-x)$%) is able to enhance the accuracy of the approximate non-integer model. Section 6 discusses the applicability and effectiveness of this identification technique on temperature-based equipment, highlighting the practical challenges of hardware implementation. Finally, Sect. 7 provides concluding remarks.

2 Theoretical background

This section introduces some fundamental definitions and notions widely applied in fractional calculus. These basic concepts can be studied in depth in various books, such as those cited in [14, 35].

Fractional calculus is conceptualized as an generalization of the classical derivative $\frac{\mathrm{d}^n}{\mathrm{d}t^n}$ to a non-integer fundamental operator ${}_aD_t^{\alpha}$. Here, $\alpha \in \mathbb{R}$ represents the fractional order, and a and t represent the lower and upper limits of the differ-integral operator, respectively. This operator is defined as follows:

$${}_aD_t^{\alpha} = \begin{cases} \frac{\mathrm{d}^{\alpha}}{\mathrm{d}t^{\alpha}}, & \alpha > 0, \\ 1, & \alpha = 0, \\ \int_a^t (\mathrm{d}\tau)^{\alpha}, & \alpha < 0, \end{cases} \tag{1}$$

Typically, α is considered a real number, although it can also be complex. In our work, we focus exclusively on the real case.

The literature contains various definitions of the non-integer order operator. A brief summary of these definitions is provided in the following, with additional details available in [14, 35].

Riemann-Liouville definition
This definition is among the most commonly employed approaches for defining fractional operators. The fractional-order integral is expressed as:

$${}_0I_t^{\alpha} f(t) = {}_0D_t^{-\alpha} f(t) = \frac{1}{\Gamma(\alpha)} \int_0^t (t-\tau)^{\alpha-1} f(\tau)\mathrm{d}\tau, \tag{2}$$

where $\Gamma(\cdot)$ is the Gamma function [14], $t \geq 0$, and $\alpha \in \mathbb{R}^+$.

Given this, the fractional derivative of $f(t)$ as defined by the Riemann-Liouville approach is:

$${}_0D_t^{\alpha} f(t) = \frac{1}{\Gamma(m-\alpha)} \frac{\mathrm{d}^m}{\mathrm{d}t^m} \int_0^t (t-\tau)^{m-\alpha-1} f(\tau)\mathrm{d}\tau, \tag{3}$$

with $t \geq 0$, $\alpha \in \mathbb{R}^+$, and $m-1 < \alpha < m$ with $m \in \mathbb{Z}^+$.

Grünwald-Letnikov definition
This differ-integral operator provides a unified framework for representing both fractional integration and differentiation. This discrete approximation to fractional derivatives and integrals is given as:

$${}_0D_t^{\alpha} f(t) = \lim_{h \to 0} \frac{1}{h^{\alpha}} \sum_{k=0}^{\infty} (-1)^k \binom{\alpha}{k} f(t-kh), \tag{4}$$

where $t \geq 0$, $\alpha < 0$ and $\alpha > 0$ represent the orders of fractional integral and derivative, respectively, $\binom{\alpha}{k}$ denotes the binomial coefficient, and h is the step size.

The Grünwald-Letnikov approach is more aligned with numerical methods and is useful for approximating fractional operators.

Note that in the above definitions (Eqs. (2), (3), and (4)), 0 and t represent the terminals of fractional differentiation or integration. As a matter of simplicity, in the following discussions, ${}_0D_t^{-\alpha}$ and ${}_0D_t^{\alpha}$ will be denoted simply as $D^{-\alpha}$ and D^{α}, respectively.

Mittag-Leffler function
The two-parameter Mittag-Leffler function, as described in [36], is defined for $z \in \mathbb{C}$ by the following expression:

$$E_{\alpha,\beta}(z) = \sum_{r=0}^{\infty} \frac{z^r}{\Gamma(\alpha r + \beta)}, \tag{5}$$

where $\Gamma(\cdot)$ represents the Gamma function [14], $\alpha \in \mathbb{R}^+$, and $\beta \in \mathbb{C}$. The function $E_{\alpha,\beta}$ is a generalization of the one-parameter Mittag-Leffler function.
For any arbitrary value of z, it is expressed as:

$$E_{\alpha}(z) = \sum_{r=0}^{\infty} \frac{z^r}{\Gamma(\alpha r + 1)}. \tag{6}$$

For $\alpha = 1$ and $\beta = 1$, this function simplifies to the exponential ($E_{1,1}(z) = E_1(z) = \exp(z)$). Thus, the Mittag-Leffler function serves as a fundamental generalization of the exponential function [37], making it essential for deriving the solution to the FFOPDT model.

Laplace transform of the Riemann-Liouville derivative
The Laplace transform of the Riemann-Liouville fractional derivative is given by:

$$\mathscr{L}\{D^{\alpha} f(t)\} = s^{\alpha} F(s) - \sum_{k=0}^{n-1} s^k \left[D^{\alpha-k-1} f(t) \right]_{t=0^+}, \tag{7}$$

where $n-1 \leq \alpha < n$ and $F(s)$ denotes the Laplace transform of $f(t)$, i.e., $F(s) = \mathscr{L}\{f(t)\}(s)$. Here, $\left[D^{\alpha-k-1} f(t) \right]_{t=0^+}$

represents the initial conditions involving $f(t)$ and its fractional derivatives at $t = 0^+$.

Zero initial conditions
Zero initial conditions refer to the assumption that the terms $\left[D^{\alpha-k-1} f(t)\right]_{t=0^+} = 0$, for all $k = 0, 1, \ldots, n-1$. Under these conditions, the Laplace transform of the fractional derivative simplifies to:

$$\mathscr{L}\{D^{\alpha} f(t)\} = s^{\alpha}\mathscr{L}\{f(t)\}. \tag{8}$$

This is analogous to the conventional integer-order derivative in Laplace transforms, where differentiating in the time domain corresponds to multiplying by s in the Laplace domain. Note that using deviation variables around the operating point is an effective practice in control systems. This approach simplifies analysis and design by allowing initial conditions in the Laplace domain to be ignored [38]. This practice is extensible to fractional-order systems.

Fractional differential equations
A fractional-order continuous-time dynamical system is described by a fractional differential equation, with its most general form given as:

$$\sum_{k=0}^{n} a_k D^{\alpha_k} y(t) = \sum_{k=0}^{m} b_k D^{\beta_k} u(t), \tag{9}$$

where $y(t)$ represents the output signal, $u(t)$ the input signal, a_k (for $k = 0, \ldots, n$) and b_k (for $k = 0, \ldots, m$) are constants, and α_k (for $k = 0, \ldots, n$) and β_k (for $k = 0, \ldots, m$) are arbitrary real or rational numbers. Without loss of generality, the parameters α_k and β_k can be organized such that $\alpha_n > \alpha_{n-1} > \cdots > \alpha_0$ and $\beta_m > \beta_{m-1} > \cdots > \beta_0$.

The fractional differential equation characterized by (9) can be defined as being of commensurate order if all derivative orders are integer multiples of a common value α, where $\alpha_k, \beta_k = k\alpha$, with $\alpha \in \mathbb{R}^+$. In this case, the system can be written as:

$$\sum_{k=0}^{n} a_k D^{k\alpha} y(t) = \sum_{k=0}^{m} b_k D^{k\alpha} u(t).$$

On the other hand, the fractional system is of incommensurate order if the fractional derivative orders do not share a common base, meaning they cannot be expressed as integer multiples of a single fractional order.

Fractional transfer functions
The transfer function is a mathematical tool that defines the connection between the input and output of a dynamic system in the Laplace domain. It is particularly useful for analyzing how a system responds to different input signals and how it behaves in terms of stability, accuracy, and speed. In fractional systems, the transfer function generalizes the classical concept by incorporating derivatives of non-integer order. This transfer function is expressed as a ratio of polynomials that may include fractional powers of the Laplace variable s.

The transfer function corresponding to the differential equation of incommensurate order (9) is expressed as follows:

$$\begin{aligned} G(s) &= \frac{\mathscr{L}\{y(t)\}}{\mathscr{L}\{u(t)\}} = \frac{Q(s)}{P(s)} \\ &= \frac{b_m s^{\beta_m} + b_{m-1} s^{\beta_{m-1}} + \cdots + b_0 s^{\beta_0}}{a_n s^{\alpha_n} + a_{n-1} s^{\alpha_{n-1}} + \cdots + a_0 s^{\alpha_0}}, \end{aligned} \tag{10}$$

where it has been considered that the polynomials $Q(s)$ and $P(s)$ have no common zeros.

In the special case where the system is of commensurate order, there exists a real number α that acts to be the highest common divisor of α_k ($k = 0, \ldots, n$) and β_k ($k = 0, \ldots, m$), with $\alpha_k = k\alpha$ and $\beta_k = k\alpha$, where $0 < \alpha < 1$ and $k \in \mathbb{Z}$. Therefore, the Equation (10) can be reformulated as follows:

$$G(s) = \frac{\mathscr{L}\{y(t)\}}{\mathscr{L}\{u(t)\}} = \frac{Q(s)}{P(s)} = \frac{\sum_{k=0}^{m} b_k s^{k\alpha}}{\sum_{k=0}^{n} a_k s^{k\alpha}}. \tag{11}$$

Stability
The transfer function $G(s)$ in (10), which is strictly proper, can consider to be BIBO stable if and only if $P(s)$ does not have any roots in the region where $\mathrm{Re}(s) \geq 0$ [15].

Furthermore, the commensurate system $G(s)$ in (11) is BIBO stable if all the roots of the characteristic equation ($P(x) = 0$), where $x = s^{\alpha}$, lie outside the region $|\arg(x)| \leq \alpha \cdot \pi/2$ [15].

Step response
The step response offers valuable insights into the dynamics of a fractional system, revealing important information about its stability, response speed, and overall behavior. Additionally, it helps determine the system's dynamic characteristics at its operating point, facilitating the design of an effective control system. To further refine the analysis of system dynamics, mathematical techniques can be applied.

Partial fraction expansion of a transfer function is a mathematical method that breaks down a rational function into a sum of simpler components. This technique simplifies the computation of the system's time response using the inverse Laplace transform.

Given that $n > m$, $G(s)$ yields a proper rational transfer function. When the roots of the characteristic equation are non-repeating, the partial fraction expansion applied in (11) takes the form:

$$G(s) = \sum_{i=1}^{n} \frac{r_i}{s^{\alpha} + \lambda_i}, \tag{12}$$

where λ_i $(i = 1, \ldots, n)$ refer to the roots of the characteristic equation and r_i $(i = 1, \ldots, n)$ denote the respective residues.

These residues r_i in fractional systems not only determine the magnitude of the response based on the poles λ_i, but also influence the rate of decay or growth of the response. This behavior deviates from an exponential dynamic due to the involvement of fractional derivatives and the Mittag-Leffler function.

In particular, to calculate the residue at a pole λ_i, the general formula remains:

$$r_i = \lim_{s \to -\lambda_i} \left((s^\alpha + \lambda_i) G(s) \right).$$

Applying the inverse Laplace transform to the transfer function (12) provides the following expression for the impulse response of the fractional system:

$$h(t) = \mathscr{L}^{-1} \left\{ \sum_{i=1}^{n} \frac{r_i}{s^\alpha + \lambda_i} \right\} (t) = \sum_{i=1}^{n} r_i t^{\alpha-1} E_{\alpha,\alpha}(-\lambda_i t^\alpha), \tag{13}$$

with $E_{\alpha,\alpha}(z)$ denoting the two-parameter Mittag-Leffler function, as given in (5).

If the right-hand side of (13) is integrated, the response to a step of Eq. (12) is expressed as follows:

$$g(t) = \sum_{i=1}^{n} r_i \frac{E_{\alpha,1}(-\lambda_i t^\alpha) - 1}{\lambda_i}, \tag{14}$$

where $E_{\alpha,1}(z) = E_\alpha(z)$ is the one-parameter Mittag-Leffler function, introduced above in (6). Note that every term of $g(t)$ in Equation (14) becomes convergent to its final value as a result of the asymptotic properties of the Mittag-Leffler function [34].

3 Overview of fractional reduced-order model estimation derived from the reaction curve

This part discusses the overall FFOPDT model identification technique, which considers three points on the process response, as proposed in [32], and is summarized below. The FFOPDT model can be defined as folows:

$$P(s) = \frac{Y_\alpha(s)}{U(s)} = \frac{K e^{-Ls}}{(1 + Ts^\alpha)}, \tag{15}$$

with the following parameters of the reduced-order fractional model: K represents the gain, T and L the time-based parameters, which are the time constant and the dead time, respectively, and the non-integer order is represented by α.

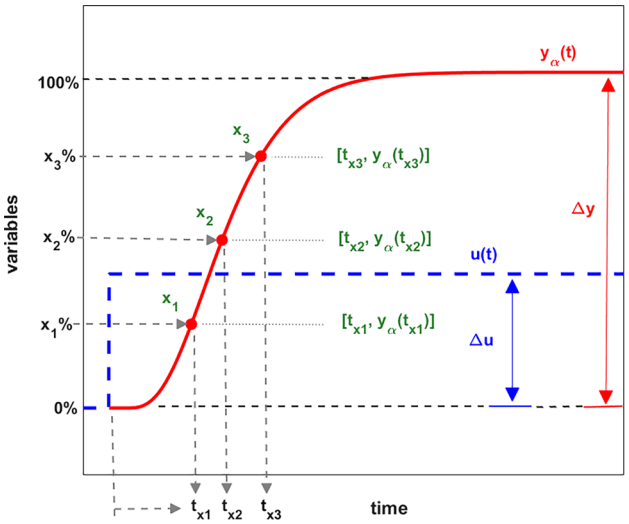

Fig. 1 Process reaction curve $y_\alpha(t)$ determined as a result of a step signal $u(t)$ and locations of the representative points

The FFOPDT model may be considered a more generalized version of the FOPDT model, which has found wide use in industry to characterize many process dynamics [39]. It is well known that the FFOPDT model can characterize the overdamped $(0 \leq \alpha \leq 1)$ and underdamped $(1 \leq \alpha \leq 2)$ behavior of the process. However, here we only focus on processes exhibiting S-shaped responses, since they are prevalent in the process industry [3]. Assuming that a variation Δu in $u(t)$ is introduced to the fractional model, the resulting output signal is $y_\alpha(t)$. Both signals are detailed in Fig. 1. Thus, the response of the model under consideration can be represented as:

$$y_\alpha(t) = \begin{cases} 0, & 0 \leq t < L \\ K \Delta u \left\{ 1 - E_\alpha \left[-\frac{1}{T}(t - L)^\alpha \right] \right\}, & t \geq L \end{cases} \tag{16}$$

with E_α being the well-known one-parameter Mittag-Leffler function [14].

The normalized and shifted time can be set as $\tau = \frac{1}{T}(t - L)^\alpha$, which is used to normalize the process response $y_\alpha(t)$ considering its variation $\Delta y = K \cdot \Delta u$. Therefore, Equation (16) can be simplified to:

$$\tilde{y}_\alpha(\tau) = \frac{y_\alpha(\tau)}{K \Delta u} = 1 - E_\alpha(-\tau), \tag{17}$$

where $0 \leq \tilde{y}_\alpha(\tau) \leq 1$ is the considered range for this variable.

From expressions (16) and (17), two significant time-based parameters can be defined for the identification procedure. More specifically, t_x denotes the time needed by the process response to achieve point x, as illustrated in Fig. 1. If expression (17) is considered, τ_x is the normalized time

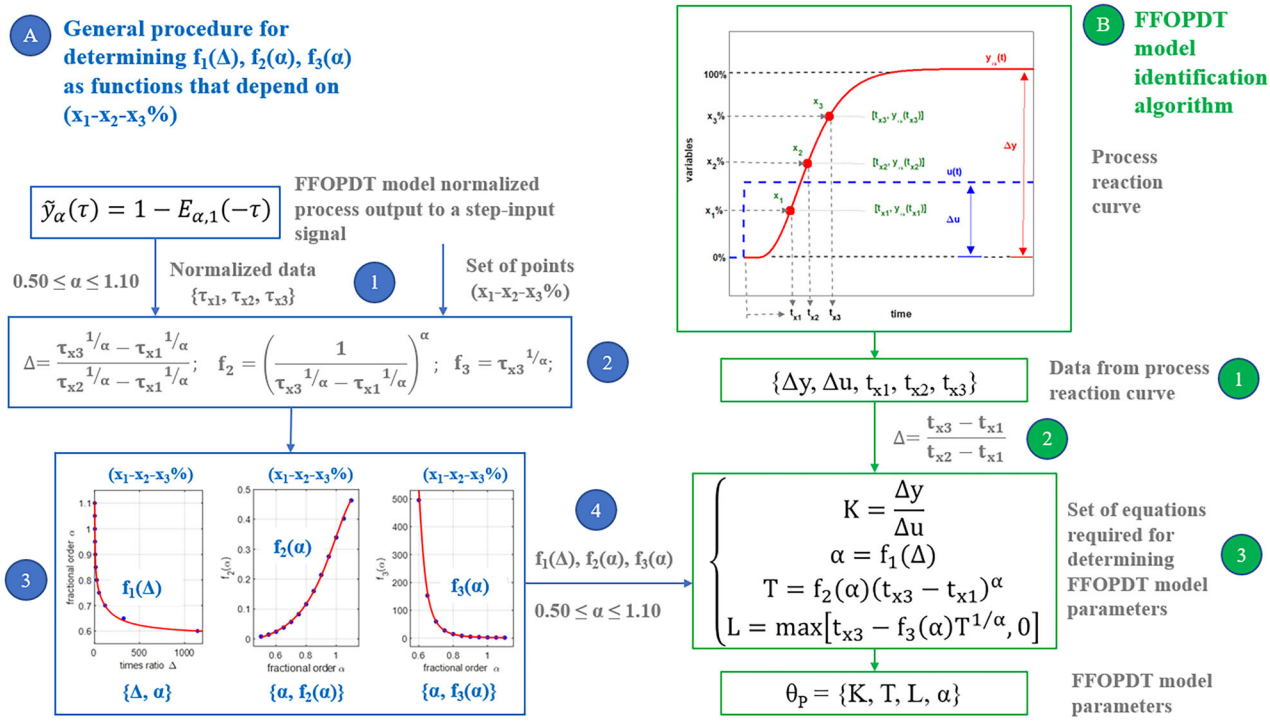

Fig. 2 Overview of the comprehensive procedure for the identification of an FFOPDT model considering three selected points. The figure also outlines the steps comprising each part of the scheme

equivalent to t_x in the domain of the normalized and shifted time variable. Therefore, the relationship between τ_x and t_x is established as follows:

$$t_x = L + (\tau_x T)^{\frac{1}{\alpha}}. \tag{18}$$

The following set of equations provide the expressions needed to derive the model parameters, which can be simply determined from the reaction curve:

$$\begin{cases} K = \frac{\Delta y}{\Delta u} \\ \alpha = f_1(\Delta) \\ T = f_2(\alpha)\left(t_{x3} - t_{x1}\right)^{\alpha} \\ L = max\left[t_{x3} - f_3(\alpha)T^{1/\alpha}, 0\right] \end{cases} \tag{19}$$

where Δu denotes the change in $u(t)$ and Δy represents the change of $y_\alpha(t)$. Here, t_{x1}, t_{x2}, and t_{x3} represent the corresponding durations to achieve x_1, x_2, and x_3% on the process response $y_\alpha(t)$, respectively. These parameters are depicted in Fig. 1. Since $\tau_{x1} < \tau_{x2} < \tau_{x3}$ and $t_{x1} < t_{x2} < t_{x3}$, $\alpha > 0$ and $T > 0$ are naturally satisfied in Equations (19). For $L \geq 0$ to be satisfied, the condition that must be fulfilled is that $t_{x3} \geq (\tau_{x3} T)^{1/\alpha}$.

Note that the corresponding functions $f_1(\Delta)$, $f_2(\alpha) = a^\alpha$ with $a = \frac{1}{\tau_{x3}^{1/\alpha} - \tau_{x1}^{1/\alpha}}$, and $f_3(\alpha) = \tau_{x3}^{1/\alpha}$, are empirically derived based on $\{\tau_{x1}, \tau_{x2}, \tau_{x3}\}$ for $0.50 \leq \alpha \leq 1.00$. To be more specific, function f_1 is dependent on the ratio index Δ, which itself depends on τ_{x1}, τ_{x2}, and τ_{x3}. Finally, functions f_2 and f_3 depend on the fractional order and τ_{x1} and τ_{x3}, and τ_{x3}, respectively.

Figure 2 schematically illustrates the proposed general identification procedure, which is composed of two parts:

Part A represents an overview of the technique used to derive the mathematical expressions for $f_1(\Delta)$, $f_2(\alpha)$, and $f_3(\alpha)$, which are dependent on x_1, x_2, and x_3. The left side of Fig. 2 illustrates the steps involved:

1. Obtain the normalized times $\{\tau_{x1}, \tau_{x2}, \tau_{x3}\}$ for the chosen points, considering the normalized process output $\tilde{y}_\alpha(\tau)$ for $0.50 \leq \alpha \leq 1.00$.
2. Determine $\{\Delta, \alpha\}$, $\{\alpha, f_2(\alpha)\}$, and $\{\alpha, f_3(\alpha)\}$ using the above normalized, where: $\Delta = \frac{\tau_{x3}^{1/\alpha} - \tau_{x1}^{1/\alpha}}{\tau_{x2}^{1/\alpha} - \tau_{x1}^{1/\alpha}}$, $f_2(\alpha) = \left(\frac{1}{\tau_{x3}^{1/\alpha} - \tau_{x1}^{1/\alpha}}\right)^{\alpha}$, and $f_3(\alpha) = \tau_{x3}^{1/\alpha}$.
3. Use a curve-fitting technique to derive functions f_1, f_2 and f_3 as rational functions.
4. Complete the set of equations (19) considering the rational expressions calculated above.

Part B illustrates the proposed identification algorithm. The right side of Fig. 2 illustrates the steps involved:

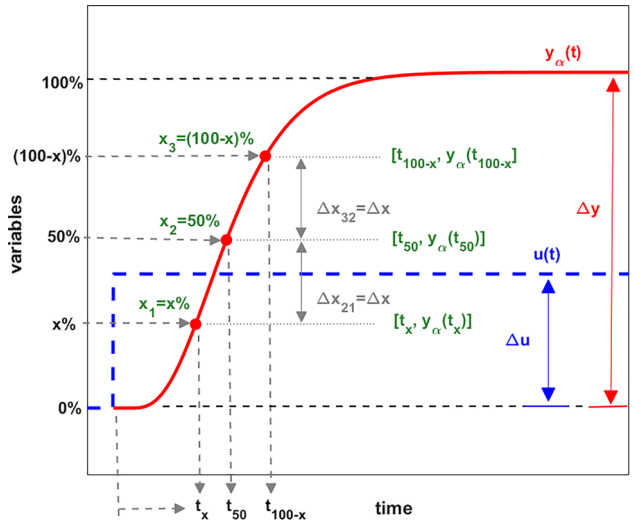

Fig. 3 Process reaction curve $y_\alpha(t)$ determined as a result of a step signal $u(t)$ and symmetrical locations

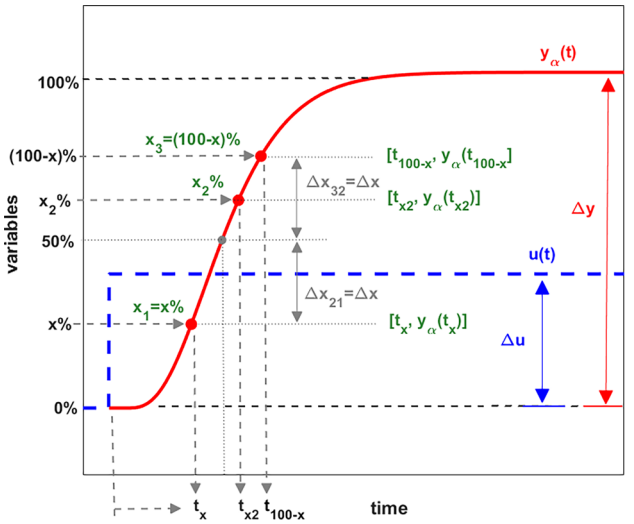

Fig. 4 Process reaction curve $y_\alpha(t)$ determined as a result of a step signal $u(t)$ and symmetrical locations

1. Obtain the necessary data for the identification technique $\{\Delta y, \Delta u, t_{x1}, t_{x2}, t_{x3}\}$.
2. Compute the ratio index, $\Delta = \frac{t_{x3}-t_{x1}}{t_{x2}-t_{x1}}$, using the corresponding times collected previously.
3. Estimate the fractional order and, thus, the corresponding values for the functions f_2 and f_3. Then, calculate θ_P employing equations in (19) and the experimental data.

For detailed information on this identification technique, readers are encouraged to consult [32].

4 Statement of the problem

The previous section presented an overview of the general approach for estimating a reduced-order fractional model, specifically the FFOPDT model, using data from a basic open-loop experiment.

Various approaches have been proposed based on the general procedure. The approach proposed in [33] consists of a straightforward simplification of this general identification technique, since it considers symmetrical points.

As shown in Fig. 3, the centroid is located at the midpoint of the process response, where $x_2 = 50\%$ with coordinates $(t_{x2} = t_{50},\ y_\alpha(t_{50}))$. The extreme points, $x_1 = x\%$ and $x_3 = (100 - x)\%$, with coordinates $(t_{x1} = t_x,\ y_\alpha(t_x))$ and $(t_{x3} = t_{100-x},\ y_\alpha(t_{100-x}))$, respectively, can be arbitrarily positioned on the reaction curve, provided they are symmetrically placed relative to the centroid $(\Delta x_{32} = \Delta x_{21} = \Delta x)$. However, reference [33] assumed that x_2 was always positioned at the midpoint of the process output $(x_2 = 50\%)$.

Therefore, given that there are techniques for identifying integer and fractional models having the centroid positioned away from the midpoint of the range, this paper examines the impact of moving the centroid x_2 along the process reaction curve, ensuring symmetry is preserved.

Figure 4 shows that the extreme points are symmetrically positioned around the midpoint of the total output range $(\Delta x_{32} = \Delta x_{21} = \Delta x)$. In contrast, the central point x_2 can be adjusted within the range $x_1 = x < x_2 < x_3 = 100 - x$, with $0 < x < 50$.

The following outlines the experimental approach used to determine the impact of x_2 on enhancing the estimated FFOPDT model's accuracy:

1. The following values $\{\tau_x, \tau_{x2}, \tau_{100-x}\}$ are obtained considering $0.50 \leq \alpha \leq 1.00$. Note that x_2 will take a set of values, $x_2 \in [x_{2,min}, \ldots, x_{2,max}]$, to assess the impact of its variation.
2. The various data collections $\{\Delta, \alpha\}$, $\{\alpha, f_2(\alpha)\}$, and $\{\alpha, f_3(\alpha)\}$ are calculated by considering the above normalized times $\{\tau_x, \tau_{x2}, \tau_{100-x}\}$.
3. The parameters $\{p_i, q_i\}$ corresponding to the functions defined in (20)-(22) are calculated through a curve-fitting procedure.

$$f_1(\Delta) = \frac{p_1\Delta^2 + p_2\Delta + p_3}{\Delta^2 + q_1\Delta + q_2}, \tag{20}$$

$$f_2(\alpha) = \frac{p_1\alpha + p_2}{\alpha^2 + q_1\alpha + q_2}, \tag{21}$$

$$f_3(\alpha) = \frac{p_1\alpha^2 + p_2\alpha + p_3}{\alpha^2 + q_1\alpha + q_2}. \tag{22}$$

4. Once these rational functions are determined, the set of Equations (19) is defined.

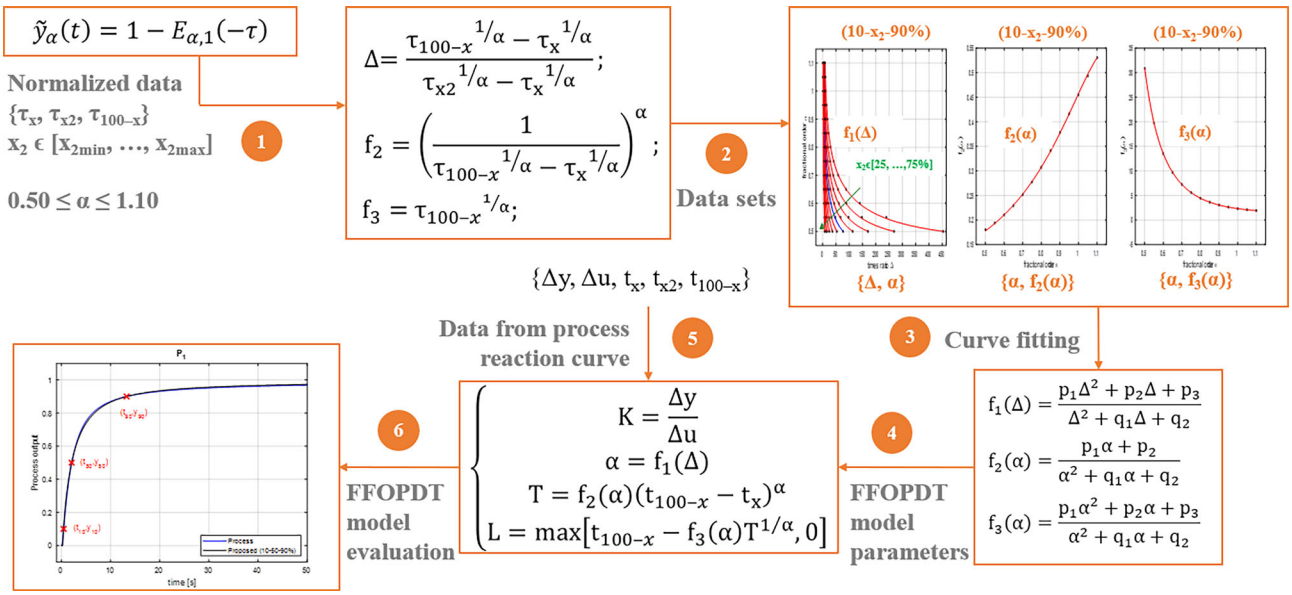

Fig. 5 Scheme of the experimental methodology used to assess the impact of adjusting x_2 on the precision of the approximate model

5. With the value of Δ for the given reaction curve, the value of α given by the function f_1 can be estimated. From this estimated value, the values of functions f_2 and f_3 can be calculated. With these, the fractional model parameters can be determined through the equations provided in (19).
6. Finally, the prediction error of the estimated model is calculated by evaluating the mean squared error (MSE) according to the following formula:

$$S(\theta) = \frac{1}{N_S}\sum_{k=1}^{N_S}[e(kT_S,\theta)]^2 = \frac{1}{N_S}\sum_{k=1}^{N_S}[y(kT_S) - y_m(kT_S,\theta)]^2, \quad (23)$$

where T_S represents the sampling interval, N_S denotes the total data points, $e(kT_s,\theta)$ is the error between the step response of the process $y(kT_S)$ and the step response of the approximate model $y_m(kT_s,\theta)$, and θ denotes the set of model parameters. Within this framework, $S_{x,y}$ is defined as the ratio between the MSE of the model derived using one identification technique and the MSE of the model estimated with a different technique. This index quantifies the performance of one identification method, expressed in terms of S, relative to another:

$$S_{x,y}(\theta_x,\theta_y) = \frac{S(\theta_x)}{S(\theta_y)}, \quad (24)$$

where $S(\cdot)$ represent the value of the performance index considered in (23), while θ_x and θ_y denote the set of parameters for two different models x and y, respectively.

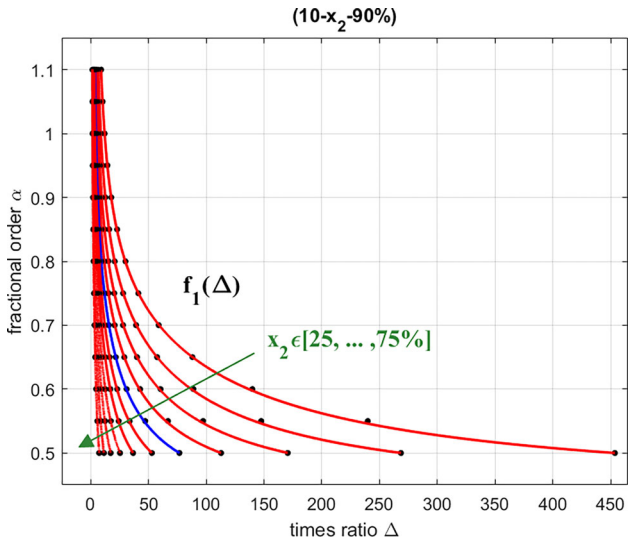

Fig. 6 Data sets $\{\Delta, \alpha\}$ and rational functions $f_1(\Delta)$, both of which depend on x_2. The curve corresponding to $x_2 = 50\%$ is shown in blue in the figure. (Color figure online)

In summary, the experimental methodology discussed is illustrated in Fig. 5.

From the data collections $\{\Delta, \alpha\}$, $\{\alpha, f_2(\alpha)\}$, and $\{\alpha, f_3(\alpha)\}$, curve-fitting results can be obtained by using the symmetrical points $(x\text{-}x_2\text{-}(100-x)\%)$.

Specifically, $x_1 = x = 10\%$, $x_2 = [25, 30, \ldots, 75\%]$, and $x_3 = 100 - x = 90\%$ are applied, where symmetry requires $\Delta x_{32} = \Delta x_{21} = \Delta x = 40\%$ for this case. Figures 6, 7 and 8 display the specified data sets along with functions f_1, f_2 and f_3 resulting from curve approximation using the Levenberg-Marquardt least-squares algorithm. The plot of

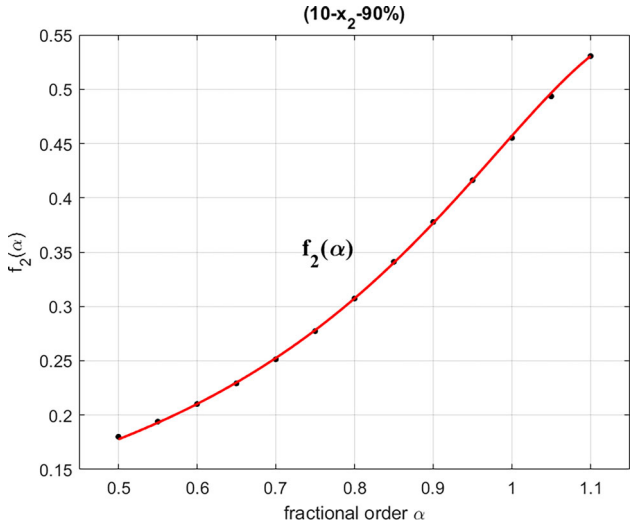

Fig. 7 Data sets $\{\alpha,\ f_2(\alpha)\}$ and rational function $f_2(\alpha)$. Note that $f_2(\alpha)$ is independent of x_2

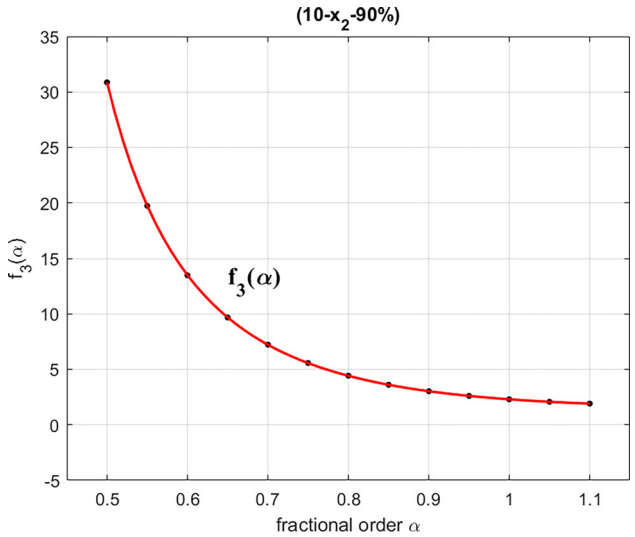

Fig. 8 Data sets $\{\alpha,\ f_3(\alpha)\}$ and rational function $f_3(\alpha)$. Note that $f_3(\alpha)$ is independent of x_2

$f_1(\Delta)$ presents a family of curves as a function of x_2, while the plots of $f_2(\alpha)$ and $f_3(\alpha)$ remain unchanged since they do not depend on x_2.

The parameters $\{p_i, q_i\}$ of the functions defined in (20)-(22) and each value $x_2 = [25, 30, \ldots, 75\%]$, calculated via curve fitting, are provided in Tables 1, 2 and 3.

The identification technique described in this paper exhibits symmetry when considering the points $(x - x_2 - (100 - x)\%)$. As a consequence of selecting $x_1 = x$ and $x_3 = 100 - x$, the range from x to $(100 - x)$ expands as x decreases, allowing the step response of the models to more accurately align with the process step response, as noted in [33]. As a result, lower values of S are achieved.

Table 1 Parameters for the rational function $f_1(\Delta)$ as a function of x_2

x_2	p_1	p_2	p_3	q_1	q_2
25%	0.4286	85.18	362.5	107.2	13.5
30%	0.4228	52.01	113.2	63.49	−31.62
35%	0.4152	34.91	38.59	41.5	−32.76
40%	0.4063	24.49	11.22	28.26	−26.71
45%	0.3965	17.62	0.7946	19.62	−20.18
50%	0.3854	12.75	−3.517	13.5	−14.93
55%	0.3720	9.265	−4.86	9.156	−10.84
60%	0.3558	6.650	−4.951	5.898	−7.648
65%	0.3351	4.698	−4.393	3.486	−5.172
70%	0.3045	3.333	−3.548	1.841	−3.347
75%	0.2590	2.282	2.712	0.5486	−1.919

Table 2 Parameters for the rational function $f_2(\alpha)$.

x_2	p_1	p_2	q_1	q_2
[25, 30, ..., 75%]	−0.0673	0.1578	−2.501	1.699

Table 3 Parameters for the rational function $f_3(\alpha)$.

x_2	p_1	p_2	p_3	q_1	q_2
[25, 30, ..., 75%]	4.066	−7.705	5.055	−0.4136	0.02868

Considering this particular set of points (10-x_2-90%), the Equations in (19) can be adapted as follows:

$$\begin{cases} K = \frac{\Delta y}{\Delta u} \\ \alpha = f_1(\Delta) \\ T = f_2(\alpha)\left(t_{90} - t_{10}\right)^{\alpha} \\ L = max\left[t_{90} - f_3(\alpha)T^{1/\alpha}, 0\right] \end{cases} \tag{25}$$

where $x_1 = x = 10\%$, $x_2 = [25, 30, \ldots, 75\%]$, and $x_3 = (100 - x) = 90\%$, and data information for the estimation of the fractional model is $\{\Delta y, \Delta u, t_{10}, t_{x2}, t_{90}\}$.

5 Illustrative examples

The FFOPDT model identification procedure outlined in Sect. 3 for symmetrical points $(x\text{-}x_2\text{-}(100 - x)\%)$ has been validated with three fractional models. As detailed in Sect. 4, the selected representative points include $x_1 = x\% = 10\%$, $x_2 \in [25, 30, \ldots, 75\%]$, and $x_3 = (100 - x)\% = 90\%$.

A key contribution of this paper demonstrates that the estimated FFOPDT model accuracy improves when x_2 is adjusted to a location other than $x_2 = 50\%$. Initially, a range of processes of fractional-order is analyzed to assess how varying x_2 influences model accuracy, considering the fractional-order interval $0.60 \leq \alpha \leq 1.00$. Subsequently,

two fractional processes of higher-order are utilized to assess the accuracy of the estimated model with $x_2 = 65\%$ and $x_2 = 50\%$, respectively. The results of the proposed method at both x_2 positions are then compared with models derived using established fractional-order identification techniques. A discussion follows to analyze the findings.

The simulations were carried out using the FOTF MATLAB Toolbox [40].

5.1 Example 1

The applied fractional model is expressed as follows:

$$P_1(s) = \frac{K_1}{(1 + T_1 s^{\lambda_i})^2} e^{-L_1 s}, \tag{26}$$

where the model parameters are: $K_1 = 1.00$, $T_1 = 1.00$ s, $L_1 = 0.10$ s, and $\lambda_i = [0.60, 0.65, 0.70, \ldots, 1.00]$.

A fractional second-order plus dead-time (FSOPDT) process is characterized by this transfer function, which introduces a structural variation compared to the reduced-order model used in the proposed identification method. Indeed, model (26) was employed in [33] using the same range: $0.60 \leq \lambda_i \leq 1.00$.

The purpose of this example is to investigate the impact of x_2 on the accuracy of the reduced-order model when the proposed identification technique is applied.

The following procedure has been applied:

1. Nine different fractional-order values have been applied to the transfer function detailed in (26). Specifically, Table 4 provides the sampling interval T_S, the total data points N_S, the computed duration $N_S T_S$, and the values of λ_i employed for the considered processes $P_{1,i}$ with $i = 1, \ldots, 9$.
2. For each process $P_{1,i}$ and each set of representative points, the fractional model parameters $\theta_{i,j} = \{K_{i,j}, T_{i,j}, L_{i,j}, \alpha_{i,j}\}$ are estimated, where $j = 1, \ldots, 11$ corresponds to each set of representative points. Table 5 lists the positions of x_2 used in the FFOPDT model identification.
3. The step response has been determined for the 99 non-integer models, and the corresponding values of $S(\theta_{i,j})$ have been calculated. Figure 9 shows all the values of $S(\theta_{i,j}) \cdot N_S$ computed for the processes $P_{1,i}$ with $i = 1, \ldots, 9$, considering x_2 positions with $j = 1, \ldots, 11$.

The resulting conclusions from Fig. 9 are as follows:

1. The highest value of $S(\theta_{i,j})$ consistently occurs at $x_2 = 25\%$ ($j = 1$).
2. As x_2 increases (i.e., for higher j values), $S(\theta_{i,j})$ shows a substantial decrease.

Table 4 Non-integer orders, sampling time, number of samples, and time duration utilized for the processes $P_{1,i}$ with i=1,…,9

i	λ_i	N_S	T_S [s]	$N_S T_S$ [s]
1	0.60	58040	0.01	580.39
2	0.65	29206	0.01	292.05
3	0.70	15816	0.01	158.15
4	0.75	8960	0.01	89.59
5	0.80	5224	0.01	52.23
6	0.85	3067	0.01	30.66
7	0.90	1761	0.01	17.60
8	0.95	965	0.01	9.64
9	1.00	594	0.01	5.93

Table 5 Symmetrical sets of points employed

j	Method #	x_2	Set of points
1	1	25%	(10–25–90%)
2	2	30%	(10–30–90%)
3	3	35%	(10–35–90%)
4	4	40%	(10–40–90%)
5	5	45%	(10–45–90%)
6	6	50%	(10–50–90%)
7	7	55%	(10–55–90%)
8	8	60%	(10–60–90%)
9	9	65%	(10–65–90%)
10	10	70%	(10–70–90%)
11	11	75%	(10–75–90%)

3. In all curves, a minimum $S(\theta_{i,j})$ is observed when $x_2 > 50\%$.
4. Specifically, for $\lambda_i \geq 0.75$, the minimum $S(\theta_{i,j})$ aligns with $x_2 = 65\%$. For $\lambda_i < 0.75$, the minimum shifts slightly below $x_2 = 65\%$, with negligible differences from that position.
5. For $\lambda_i < 0.8$, $S(\theta_{i,j})$ rises significantly from its minimum. However, this increase is minor for $\lambda_i \geq 0.8$.

These findings suggest that the accuracy of the approximate fractional model improves when using the FFOPDT identification technique with symmetrical points, particularly when the central point x_2 is located around 65%. Figure 10 presents the relative performance index values comparing methods #9 and #6 ($x_2 = 65\%$ and $x_2 = 50\%$), respectively, based on the values of λ_i with $i = 1, \ldots, 9$. The figure demonstrates that for all fractional orders λ_i considered in process (26), the proposed identification technique with $x_2 = 65\%$ yields significant improvements in model accuracy compared to $x_2 = 50\%$.

For illustration, the case $i = 5$ ($\lambda_5 = 0.80$) for the processes $P_{1,i}$, as analyzed in [33] under symmetrical con-

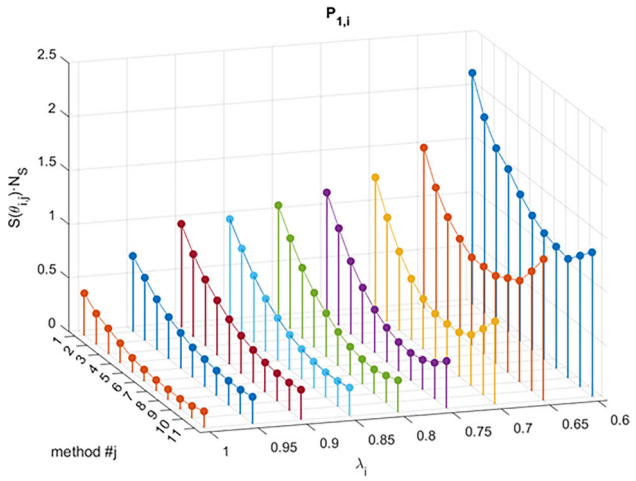

Fig. 9 Performance index $S(\theta_{i,j})$ multiplied by N_S calculated for the 99 FFOPDT models estimated using the proposed procedure. The model parameters $\theta_{i,j}$ are defined based on processes $P_{1,i}$ with $i = 1, \ldots, 9$ and locations x_2 with $j = 1, \ldots, 11$

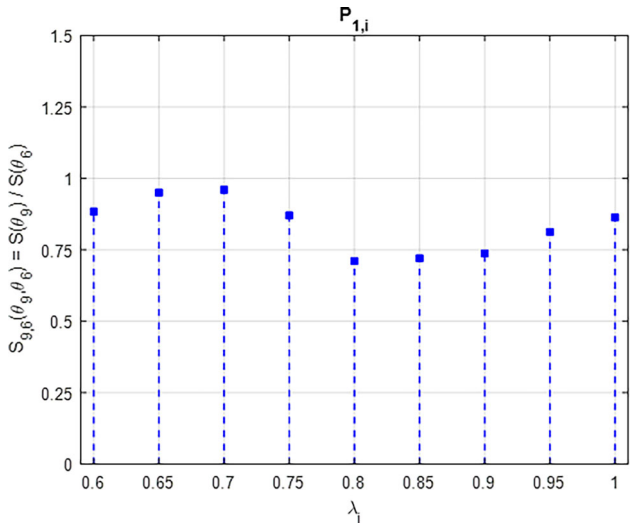

Fig. 10 $S_{9,6}(\theta_9, \theta_6)$ represent the relative performance values considering each process $P_{1,i}$ $(i = 1, \ldots, 9)$ with fractional orders λ_i. These values represent the ratio of performance between the method with $x_2 = 65\%$ (#9) and the method with $x_2 = 50\%$ (#6)

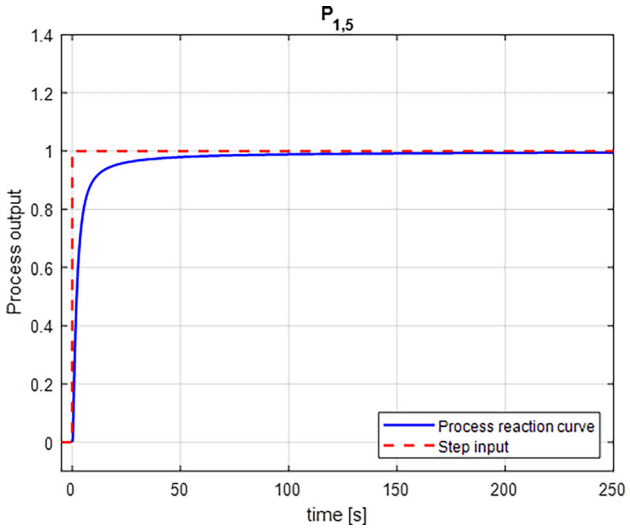

Fig. 11 Step response curve for the process $P_{1,5}$ and input signal

Table 6 Process information required for the process $P_{1,5}$

Method #6		Method #9
	$\Delta u = 1.00$	
	$\Delta y = 1.00$	
	$t_{10} = 0.4890$ s	
$t_{50} = 1.9900$ s		$t_{65} = 2.6250$ s
	$t_{90} = 9.7230$ s	

Table 7 FFOPDT model parameters identified using the proposed method with sets of points (10–50–90%) and (10–65–90%) for the process $P_{1,5}$

Method #6	Method #9
$K_{5,6} = 1.00$	$K_{5,9} = 1.00$
$T_{5,6} = 2.2003$ s	$T_{5,9} = 2.0448$ s
$L_{5,6} = 0.3466$ s	$L_{5,9} = 0.3629$ s
$\alpha_{5,6} = 0.8447$	$\alpha_{5,9} = 0.8274$

ditions, is examined below. Figure 11 illustrates the step response of process $P_{1,5}$. The process data required for identification and the respective model parameters $\theta_{5,j} = \{K_{5,j}, T_{5,j}, L_{5,j}, \alpha_{5,j}\}$ are presented in Tables 6 and 7 for cases $j = 6$ $(x_2 = 50\%)$ and $j = 9$ $(x_2 = 65\%)$. The results obtained using the (10–50–90%), as suggested in [33], are compared with those with (10–65–90%), which yield the minimum S value.

Figures 12 and 13 display the responses to a step of the approximate fractional models with parameters $\theta_{5,6}$ and $\theta_{5,9}$, estimated using the proposed technique for (10–50–90%) and (10–65–90%), respectively. Although good results are obtained in both cases when compared to the reaction curve, the model with $x_2 = 65\%$ performs better than the one with $x_2 = 50\%$. In particular, $S(\theta_{5,6}) = 6.06 \cdot 10^{-5}$ for $x_2 = 50\%$ while $S(\theta_{5,9}) = 4.31 \cdot 10^{-5}$ for $x_2 = 65\%$, indicating a 30% reduction in S and resulting in a more accurate model with $x_2 = 65\%$.

To assess the impact of x_2's position on model accuracy, Fig. 14 shows the $S(\theta_{5,j})$ values for the 11 methods $(j = 1, \ldots, 11)$, with x_2 ranging from 25% to 75%. The results indicate that the minimum $S(\theta_{5,j})$ value occurs for $j = 9$, corresponding to $x_2 = 65\%$.

Figure 15 presents the values of $S_{9,j}(\theta_{5,9}, \theta_{5,j}) = S(\theta_{5,9})/S(\theta_{5,j})$ for each x_2 location $(j = 1, \ldots, 11)$ defined in Table 5. This comparison quantifies the advantage of selecting

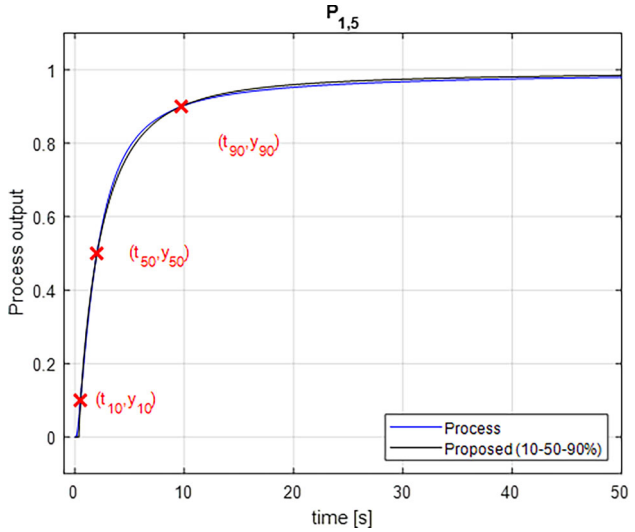

Fig. 12 Step response of the FFOPDT model identified by employing developed technique with $x_2 = 50\%$ (method #6)

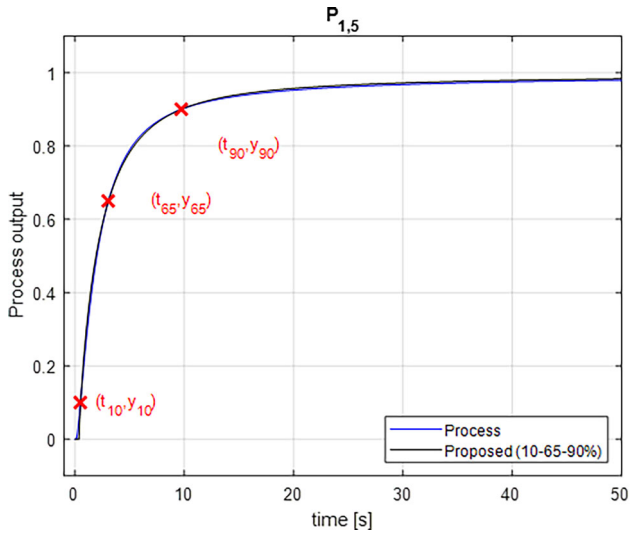

Fig. 13 Step response of the FFOPDT model identified by employing developed technique with $x_2 = 65\%$ (method #9)

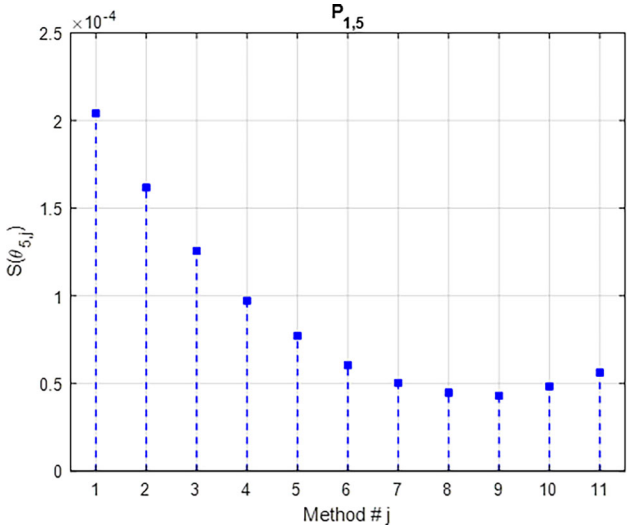

Fig. 14 Values of $S(\theta_{5,j})$ calculated using techniques #1-11 for the process $P_{1,5}$

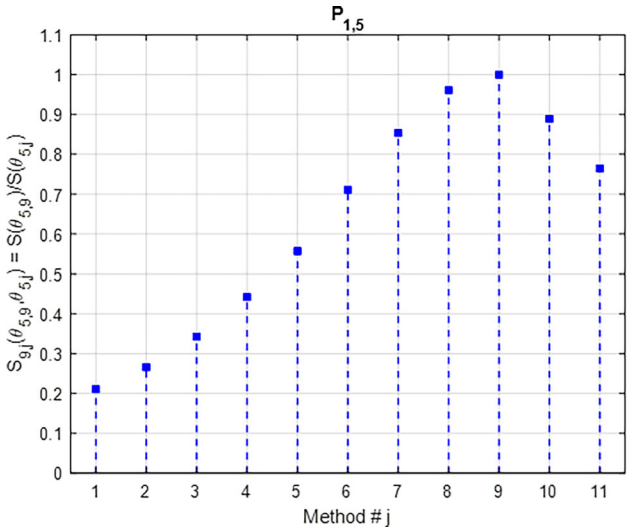

Fig. 15 Relative performance values $S_{9,j}$ calculated using techniques #1-11 with respect to the one calculated using method #9 for the process $P_{1,5}$

$x_2 = 65\%$ ($j = 9$) with the chosen identification technique relative to all other x_2 positions. For values of $x_2 < 65\%$, the benefit of using $x_2 = 65\%$ increases steadily, reaching up to an 80% improvement compared to $x_2 = 25\%$. Similarly, for $x_2 > 65\%$, $x_2 = 65\%$ still offers a 25% advantage compared to $x_2 = 75\%$.

Fractional-order model identification methods are known to yield better performance index S values compared to integer-order methods. Previous work [33] demonstrated that the fractional model obtained using (10–50–90%) outperforms widely used integer-order models for the same example. Since the FFOPDT model with $x_2 = 65\%$ achieves higher accuracy than with $x_2 = 50\%$, the findings from [33] are also applicable in this context.

5.2 Example 2

A higher-order non-integer transfer function exhibiting dominant lag characteristics is utilized in this subsection:

$$P_2(s) = \frac{K_2}{(1 + T_2 s^{\lambda_2})^n}, \tag{27}$$

where the parameters are $K_2 = 2.00$, $T_2 = 1.00$ s, $n = 5$, and $\lambda_2 = 0.85$.

This model, originally proposed in [25] and subsequently used in [33] as a demonstrative example, validated the performance for the FFOPDT identification technique considering symmetrical points.

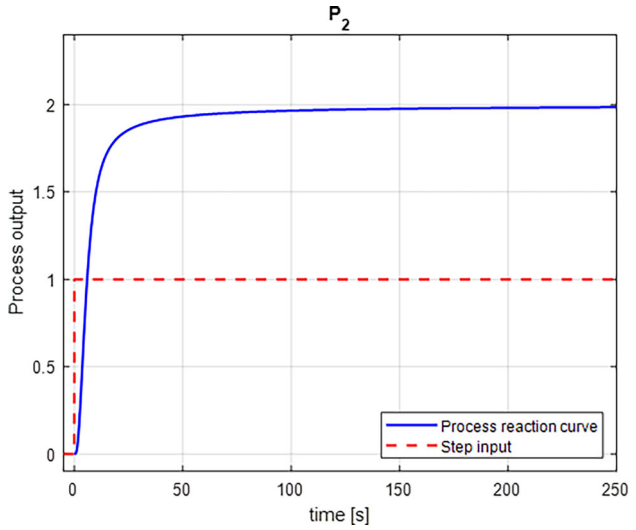

Fig. 16 Step response curve for the process P_2 and input signal

Table 8 Process information required for the process P_2

Method #6		Method #9
	$\Delta u = 1.00$	
	$\Delta y = 2.00$	
	$t_{10} = 2.3450$ s	
$t_{50} = 5.8450$ s		$t_{65} = 7.8050$ s
	$t_{90} = 19.2050$ s	

Table 9 FFOPDT model parameters identified employing the developed technique with set of points (10–50–90%) and (10–65–90%) for the process P_2

Method #6	Method #9
$K_{2,6} = 2.00$	$K_{2,9} = 2.00$
$T_{2,6} = 5.0713$ s	$T_{2,9} = 4.3409$ s
$L_{2,6} = 1.8860$ s	$L_{2,9} = 1.9975$ s
$\alpha_{2,6} = 0.9119$	$\alpha_{2,9} = 0.8798$

Here, the fractional model estimated for $x_2 = 65\%$ using this identification approach is compared to models obtained with $x_2 = 50\%$ and other models derived from alternative identification methods.

Figure 16 presents the open-loop step response for process P_2. From these results, Table 8 summarizes the process data required for FFOPDT identification procedures using the sets (10–50–90%) and (10–65–90%). Table 9 lists the corresponding parameters $\theta_{2,j} = \{K_{2,j}, T_{2,j}, L_{2,j}, \alpha_{2,j}\}$ for methods $j = 6$ (with $x_2 = 50\%$) and $j = 9$ (with $x_2 = 65\%$), while Table 10 shows the models estimated using the three approaches in [25], with fractional model parameters $\theta_{2,j}$ for $j = 12, 13, 14$, representing methods #12-14.

Table 10 FFOPDT model parameters determined by employing the various strategies suggested in [25] for the process P_2

Method #12 (strategy 1)	Method #13 (strategy 2)	Method #14 (strategy 3)
$K_{2,12} = 2.00$	$K_{2,13} = 2.00$	$K_{2,14} = 2.00$
$T_{2,12} = 5.00$ s	$T_{2,13} = 5.00$ s	$T_{2,14} = 4.48$ s
$L_{2,12} = 1.50$ s	$L_{2,13} = 0.69$ s	$L_{2,14} = 1.50$ s
$\alpha_{2,12} = 0.85$	$\alpha_{2,13} = 0.85$	$\alpha_{2,14} = 0.85$

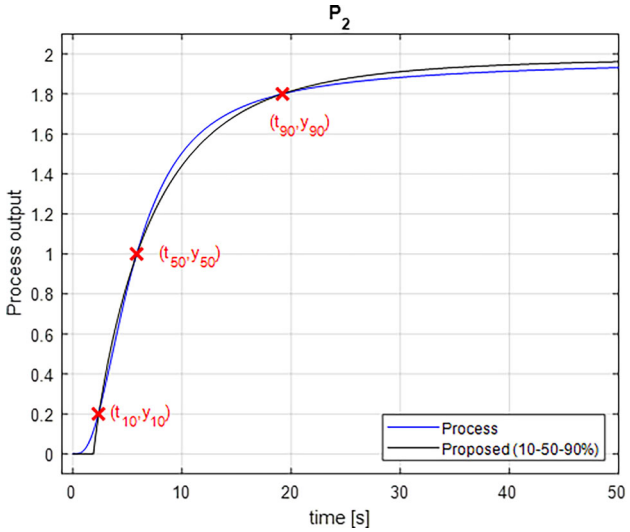

Fig. 17 Step response of the FFOPDT model identified by employing the developed technique with $x_2 = 50\%$ (method #6) for the process P_2

Figures 17, 18, 19, 20 and 21 show the step responses of the fractional models estimated using methods #6 ($x_2 = 50\%$), #9 ($x_2 = 65\%$), and #12-14, respectively, along with the reaction curve.

To assess model accuracy, Table 11 provides values of the performance index $S(\theta_{2,j})$ for each model estimated by these procedures ($j = 1, \ldots, 14$) applied to P_2.

The relative performance index $S_{9,j}(\theta_{2,9}, \theta_{2,j})$, comparing models from methods #1-14 to method #9 (with $x_2 = 65\%$), is shown in Table 12. Here, $\theta_{2,9}$ is the parameter vector obtained from method #9 for process P_2, while $\theta_{2,j}$ corresponds to method #j, with $j = 1, \ldots, 14$. Figures 22 and 23 visualize this data.

Figure 22 shows $S_{9,j}$ values for models estimated by techniques #1-11, with $j = 1, \ldots, 11$, compared to technique #9. The index S increases significantly up to 80% for $x_2 = 25\%$. For $x_2 > 65\%$, the values of S at $x_2 = 70\%$ are similar to those at 65%, with a slight increase of up to 11% at $x_2 = 75\%$. Figure 23 presents values of $S_{9,j}$ for models estimated using techniques #6, #12, #13, and #14. The results show that method #9 ($x_2 = 65\%$) reduces S by 36% com-

Table 11 Performance index $S(\theta_{2,j})$ computed for the FFOPDT models determined employing the identification techniques considered with $j = 1, \ldots, 14$ for the process P_2

j	Method	Model	x_2 (%)	set of points	$S(\theta_{2,j})$
1	#1	FFOPDT	25	(10–25–90%)	1.50×10^{-3}
2	#2	FFOPDT	30	(10–30–90%)	1.10×10^{-3}
3	#3	FFOPDT	35	(10–35–90%)	9.01×10^{-4}
4	#4	FFOPDT	40	(10–40–90%)	7.09×10^{-4}
5	#5	FFOPDT	45	(10–45–90%)	5.56×10^{-4}
6	#6	FFOPDT	50	(10–50–90%)	4.49×10^{-4}
7	#7	FFOPDT	55	(10–55–90%)	3.66×10^{-4}
8	#8	FFOPDT	60	(10–60–90%)	3.13×10^{-4}
9	#9	FFOPDT	65	(10–65–90%)	2.86×10^{-4}
10	#10	FFOPDT	70	(10–70–90%)	2.89×10^{-4}
11	#11	FFOPDT	75	(10–75–90%)	3.22×10^{-4}
12	Tavakoli-Kakhki 1	FFOPDT	–	–	1.10×10^{-3}
13	Tavakoli-Kakhki 2	FFOPDT	–	–	1.90×10^{-3}
14	Tavakoli-Kakhki 3	FFOPDT	–	–	6.56×10^{-4}
		$N_S = 25,001$			

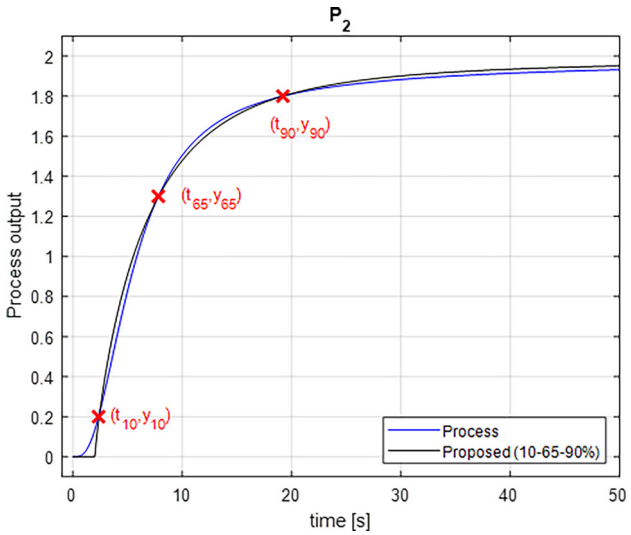

Fig. 18 Step response of the FFOPDT model identified by employing the developed technique with $x_2 = 65\%$ (method #9) for the process P_2

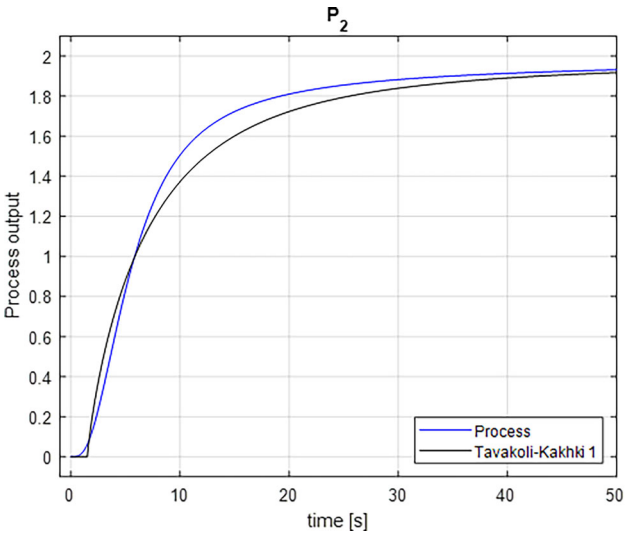

Fig. 19 Step response of the FFOPDT model identified by employing the approach outlined in [25] (strategy 1) for the process P_2

pared to method #6 ($x_2 = 50\%$), and by 75%, 85%, and 56%, respectively, compared to methods #12, #13, and #14.

Thus, this example also demonstrates that moving x_2 to a value around 65% can substantially enhance the accuracy of the FFOPDT model.

5.3 Example 3

This subsection utilizes a higher-order non-integer transfer function:

$$P_3(s) = \frac{K_3}{\prod_{i=1}^{3}(1 + T_i s^{\lambda_3})}, \tag{28}$$

where $K_3 = 3.00$, $T_1 = 3.00$ s, $T_2 = 2.00$ s, $T_3 = 1.00$ s, and $\lambda_3 = 0.88$.

This model, originally proposed in [25] and also applied in [32] as a demonstrative example, validated the performance of the FFOPDT model identification technique with symmetrical and asymmetrical points. The FFOPDT model estimated with this identification approach for $x_2 = 65\%$ is compared to the one obtained for $x_2 = 50\%$ and with models estimated using alternative identification techniques.

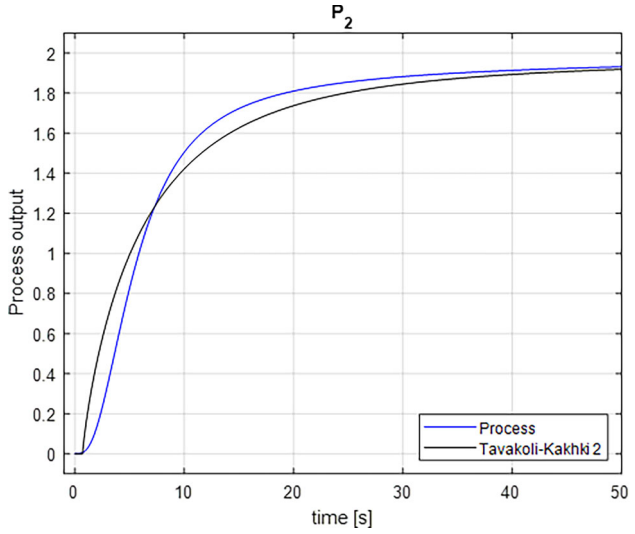

Fig. 20 Step response of the FFOPDT model identified by employing the approach outlined in [25] (strategy 2) for the process P_2

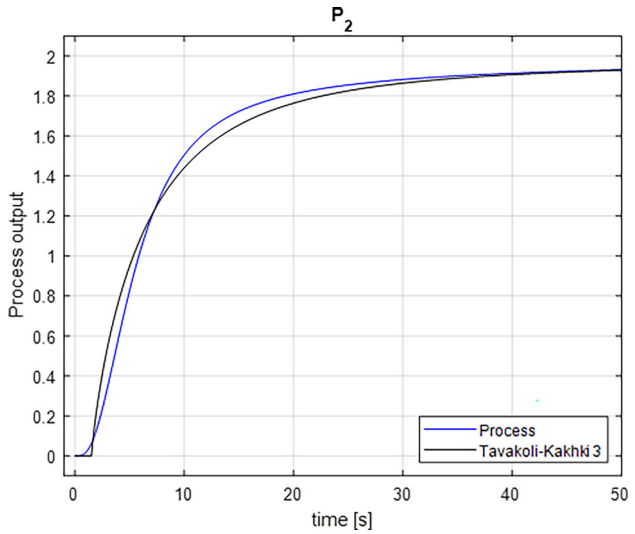

Fig. 21 Step response of the FFOPDT model identified by employing the approach outlined in [25] (strategy 3) for the process P_2

Table 12 Relative performance values comparing different fractional-order models for the process P_2

Compared methods	$S_{9,j} = S_9/S_j$	Improvement (%)
#9 - #1	0.1976	80.2
#9 - #2	0.2499	75.0
#9 - #3	0.3182	68.2
#9 - #4	0.4047	59.5
#9 - #5	0.5156	48.4
#9 - #6	0.6391	36.1
#9 - #7	0.7832	21.7
#9 - #8	0.9176	8.2
#9 - #9	1.0000	–
#9 - #10	0.9927	1.0
#9 - #11	0.8910	10.9
#9 - #12	0.2501	75.0
#9 - #13	0.1526	84.7
#9 - #14	0.4369	56.3

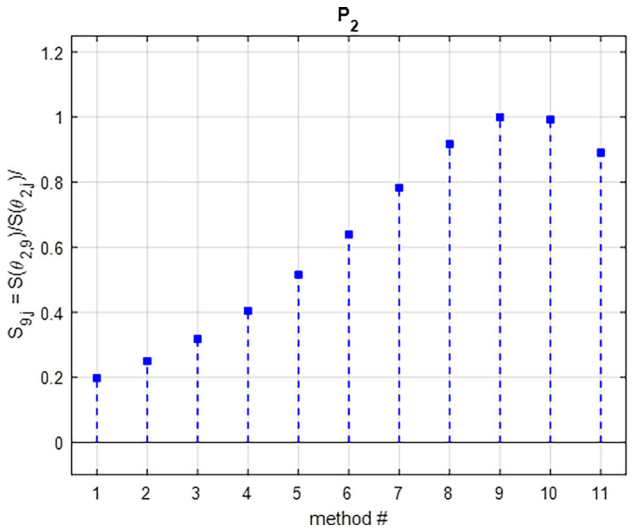

Fig. 22 Relative performance values calculated using techniques #1-11 with respect to the one calculated using technique #9 for the process P_2

Figure 24 illustrates the step input applied to process P_3 and the corresponding model response. Table 13 provides an overview of the process data needed for FFOPDT identification, using the set of points (10–50–90%) and (10–65–90%). Table 14 lists $\theta_{3,j} = \{K_{3,j}, T_{3,j}, L_{3,j}, \alpha_{3,j}\}$ considering methods $j = 6$ ($x_2 = 50\%$) and $j = 9$ ($x_2 = 65\%$). Process (28) is also estimated using an FFOPDT model derived from the technique proposed in [25], an FFOPDT model derived through the optimization method in [18], and an optimal FOPDT model. The estimated parameters $\theta_{3,j}$ for methods #12-14 are provided in Table 15.

Figures 25 and 26 display the step responses of the approximate models estimated employing techniques #6 ($x_2 = 50\%$) and #9 ($x_2 = 65\%$), as well as the reaction curve, respectively. Symmetrical points (x-x_2-$(100-x)\%$) are also included. Additionally, Figs. 27, 28 and 29 present the step response of the process P_3, along with the step responses of reduced-order models based on Tavakoli-Kakhki's (method #12) and Guevara et al.'s (method #13) approaches, as well as the optimal FOPDT model (method #14).

To assess the accuracy of these models, Table 16 displays the index values $S_{3,j}$ for the approximate models derived employing techniques ($j = 1, \ldots, 14$) applied to process P_3.

Figure 30 demonstrates that increasing x_2 to approximately 65% improves the accuracy of the estimated FFOPDT

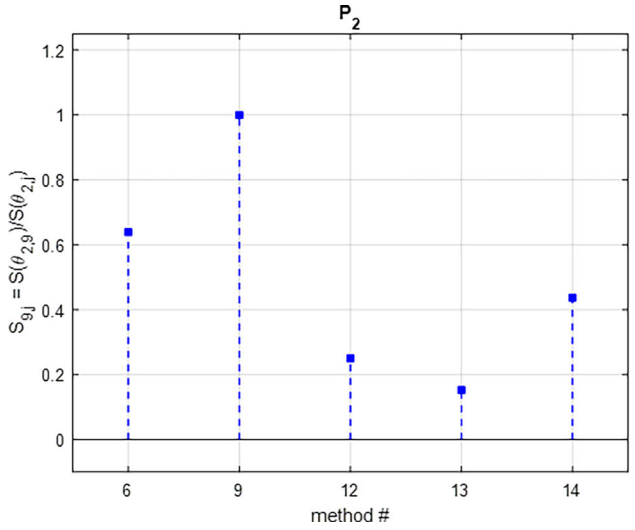

Fig. 23 Relative performance values calculated using techniques #6 and #12-14 with respect to the one calculated using technique #9 for the process P_2

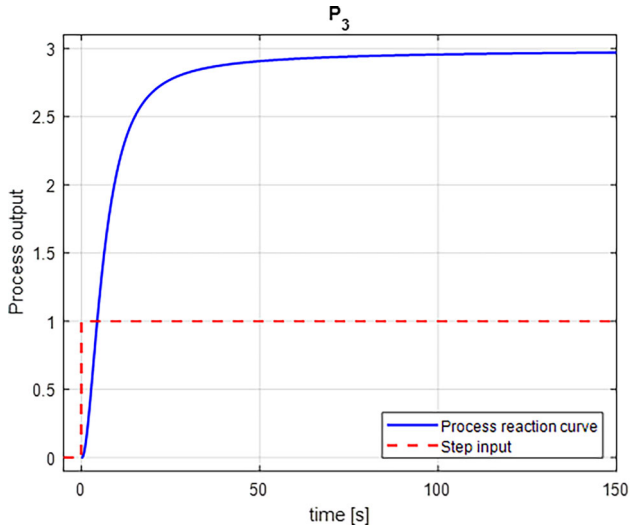

Fig. 24 Step response curve for the process P_3 and input signal

Table 13 Process information required for the process P_3

Method #6	Method #9
$\Delta u = 1.00$	
$\Delta y = 3.00$	
$t_{10} = 2.0290$ s	
$t_{50} = 6.3850$ s	$t_{65} = 8.8640$ s
$t_{90} = 20.8030$ s	

model. Beyond this point, further increases in x_2 do not yield additional benefits.

Figure 31 presents a comparison of $S(\theta_{3,j})$ values with techniques #6, #9, #12, #13, and #14 ($j = 6, 9, 12, 13, 14$). The results indicate that method #14, representing the optimal FOPDT model, exhibits significantly reduced accuracy compared to the FFOPDT model. Among all methods, method #9 ($x_2 = 65\%$) achieves the best results, even outperforming optimization-based methods #13 and #14.

Table 14 FFOPDT model parameters identified employing the developed technique with sets of points (10–50–90%) and (10–65–90%) for the process P_3

Method #6	Method #9
$K_{3,6} = 3.00$	$K_{3,9} = 3.00$
$T_{3,6} = 6.6709$ s	$T_{3,9} = 5.9386$ s
$L_{3,6} = 1.3436$ s	$L_{3,9} = 1.4627$ s
$\alpha_{3,6} = 0.9477$	$\alpha_{3,9} = 0.9240$

Table 15 FFOPDT model parameters determined with the identification methods outlined in [25], in [18], and with the optimal parameters of an FOPDT model for the process P_3

Method #12	Method #13	Method #14
$K_{3,12} = 3.00$	$K_{3,13} = 3.00$	$K_{3,14} = 3.00$
$T_{3,12} = 6.30$ s	$T_{3,13} = 5.63$ s	$T_{3,14} = 8.74$ s
$L_{3,12} = 1.00$ s	$L_{3,13} = 1.88$ s	$L_{3,14} = 0.00$ s
$\alpha_{3,12} = 0.9200$	$\alpha_{3,13} = 0.9263$	–

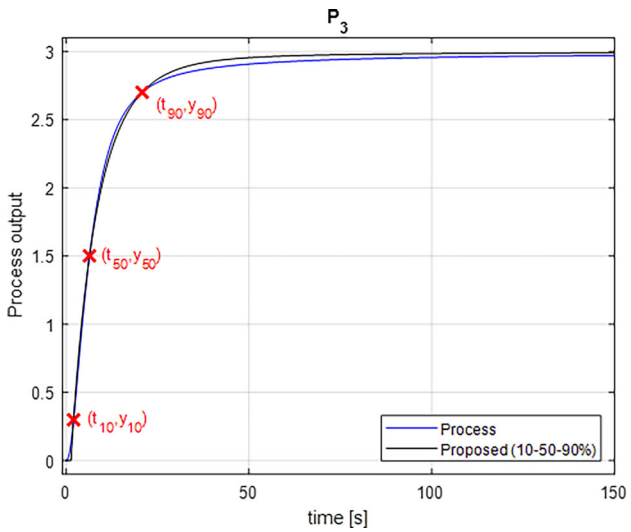

Fig. 25 Step response of the FFOPDT model identified by employing the developed technique with $x_2 = 50\%$ (method #6) for the process P_3

The index $S_{9,j}(\theta_{3,9}, \theta_{3,j})$, comparing methods #1-14 to method #9 ($x_2 = 65\%$), is listed in Table 17. Here, $\theta_{3,9}$ denotes the model parameter vector obtained from method #9 for process P_3, while $\theta_{3,j}$ represents the parameters derived from method #j ($j = 1, \ldots, 14$) for process P_3. This data is illustrated in Figs. 32 and 33.

Figure 32 shows the $S_{9,j}$ values for techniques #1-11 ($j = 1, \ldots, 11$) compared to #9, revealing that S increases sharply

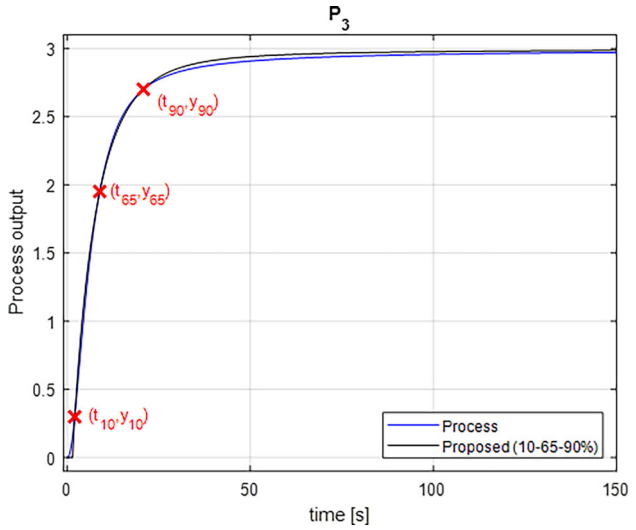

Fig. 26 Step response of the FFOPDT model identified by employing the developed technique with $x_2 = 65\%$ (method #9) for the process P_3

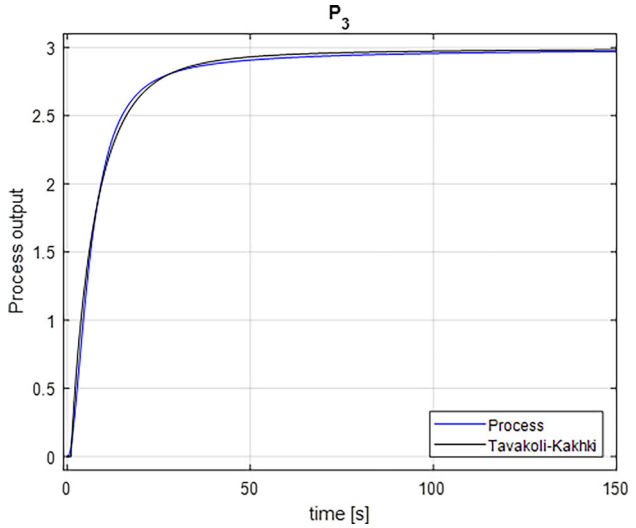

Fig. 27 Step response of the FFOPDT model identified by employing the approach outlined in [25] for the process P_3

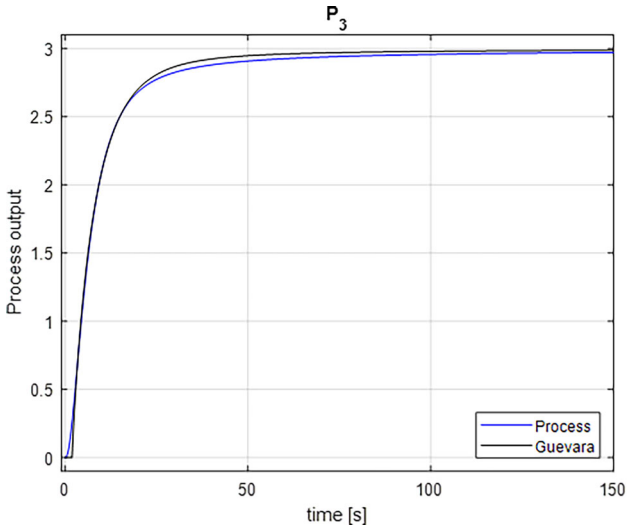

Fig. 28 Step response of the FFOPDT model identified by employing the approach outlined in [18] for the process P_3

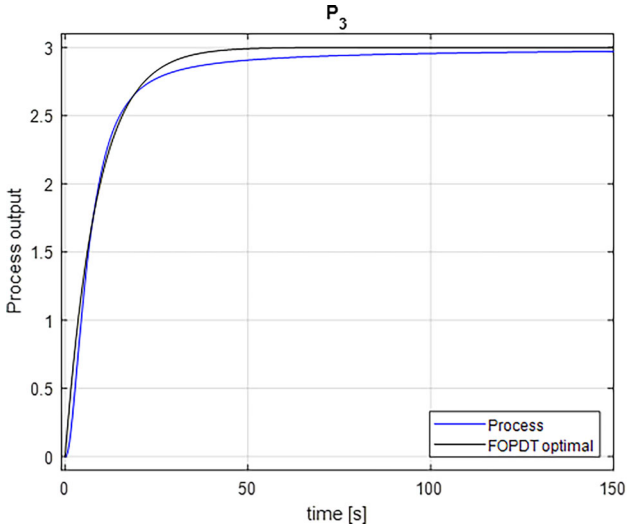

Fig. 29 Step response of the optimal FOPDT model for the process P_3

to nearly 80% for $x_2 = 25\%$ when $x_2 < 65\%$. For $x_2 \geq 65\%$, the S values remain similar, indicating no significant benefit in further increasing x_2.

Figure 33 shows $S_{9,j}$ values for techniques #6, #12, #13, and #14 compared to #9. Method #9 ($x_2 = 65\%$) reduces S by 33.9% compared to method #6 ($x_2 = 50\%$), and by 36.4%, 23.8%, and 83.8% compared to models #12, #13, and #14, respectively. This example also demonstrated that setting x_2 to approximately 65% can significantly improve the accuracy of the fractional model.

5.4 Discussion

A variety of non-integer process models was employed to evaluate the performance of the proposed identification technique for estimating FFOPDT models and to investigate how adjusting x_2 in the representative points (x-x_2-$(100 - x)\%$) affects the accuracy of the approximate model. This study specifically focuses on identifying processes with fractional-order behavior, with the FFOPDT model order constrained to $0.50 \leq \alpha \leq 1.00$. Such processes are commonly encountered in process control [3].

For the academic community, it is widely known that the accuracy of the estimated fractional model is influenced by the positions of selected points along the process reaction curve [2]. In traditional identification techniques for integer-

Table 16 Performance index $S(\theta_{3,j})$ computed for the FFOPDT models determined employing the identification techniques considered with $j = 1, \ldots, 14$ for the process P_3.

j	Method	Model	x_2 (%)	Set of points	$S(\theta_{3,j})$
1	#1	FFOPDT	25	(10–25–90%)	3.80×10^{-3}
2	#2	FFOPDT	30	(10–30–90%)	3.00×10^{-3}
3	#3	FFOPDT	35	(10–35–90%)	2.40×10^{-3}
4	#4	FFOPDT	40	(10–40–90%)	2.00×10^{-3}
5	#5	FFOPDT	45	(10–45–90%)	1.60×10^{-3}
6	#6	FFOPDT	50	(10–50–90%)	1.30×10^{-3}
7	#7	FFOPDT	55	(10–55–90%)	1.10×10^{-3}
8	#8	FFOPDT	60	(10–60–90%)	9.55×10^{-4}
9	#9	FFOPDT	65	(10–65–90%)	8.65×10^{-4}
10	#10	FFOPDT	70	(10–70–90%)	8.44×10^{-4}
11	#11	FFOPDT	75	(10–75–90%)	8.68×10^{-4}
12	Tavakoli-Kakhki	FFOPDT	–	–	1.40×10^{-3}
13	Guevara	FFOPDT	–	–	1.10×10^{-3}
14	Optimal	FOPDT	–	–	5.30×10^{-3}
		$N_S = 15,001$			

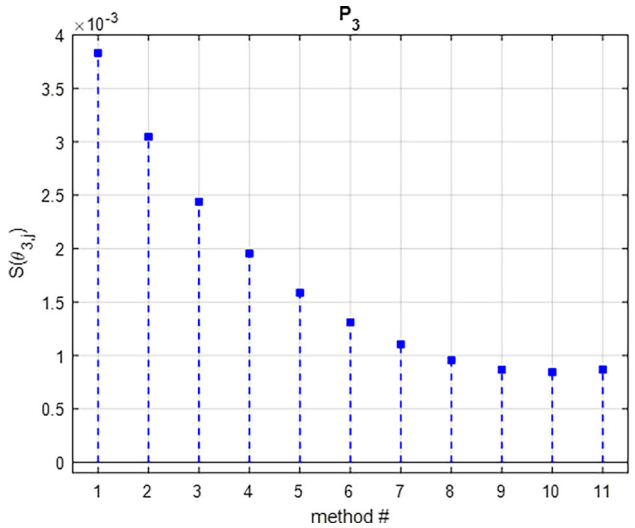

Fig. 30 Values of $S(\theta_{3,j})$ calculated using methods #1-11 for the process P_3

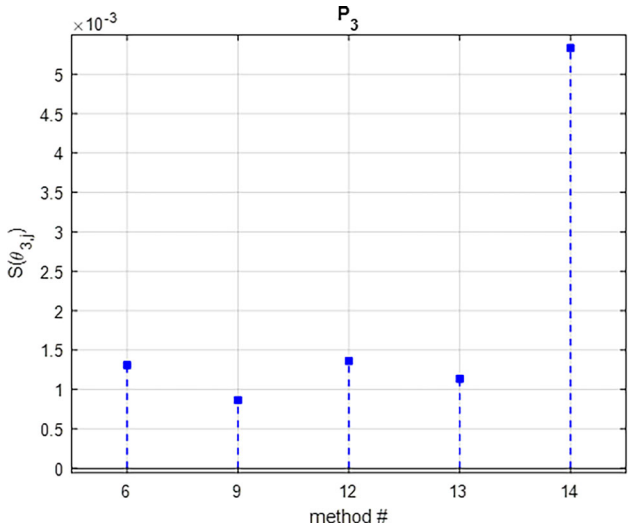

Fig. 31 Values of $S(\theta_{3,j})$ calculated using techniques #6, #9, and #12-14 for the process P_3

order models, however, the selection of these points is often quite arbitrary. In some cases, no rationale is provide for their selection [6], while for others, key points are chosen based on their relationship to model parameters [5]. Some methods strategically select these points to optimize parameter accuracy [4]. In contrast, fractional-order identification techniques provide well-documented insights into the influence of representative points, showing that both asymmetrical and symmetrical sets impact model accuracy [32], with a particular emphasis on symmetrical sets in [41].

This study focuses exclusively on the symmetrical case described in [33]. Considering the symmetry requirements, the representative points (x_1-x_2-x_3%) are chosen by optimally positioning one point ($x_1 = x\%$), while the opposing point is defined symmetrically ($x_3 = (100 - x)\%$). The primary aim of this paper is thus to locate the optimal placement of the central point, x_2.

A key finding is the validation of the estimated model's accuracy and sensitivity in relation to the positions of the three selected points. In particular, significant improvements in model accuracy are achieved by placing x_2 at a location different from $x_2 = 50\%$, while preserving symmetry and fixed positions for x_1 and x_3. Specifically, as discussed in Sect. 5, the accuracy of the identified model reaches a minimum value for $x_2 > 50$, with the optimal position consistently observed

Table 17 Relative performance values comparing different fractional-order models for the process P_3

Compared methods	$S_{9,j} = S_9/S_j$	Improvement (%)
#9 - #1	0.2259	77.4
#9 - #2	0.2842	71.6
#9 - #3	0.3549	64.5
#9 - #4	0.4430	55.7
#9 - #5	0.5457	45.4
#9 - #6	0.6609	33.9
#9 - #7	0.7844	21.6
#9 - #8	0.9058	9.4
#9 - #9	1.0000	–
#9 - #10	1.0257	–
#9 - #11	0.9971	–
#9 - #12	0.6359	36.4
#9 - #13	0.7623	23.8
#9 - #14	0.1623	83.8

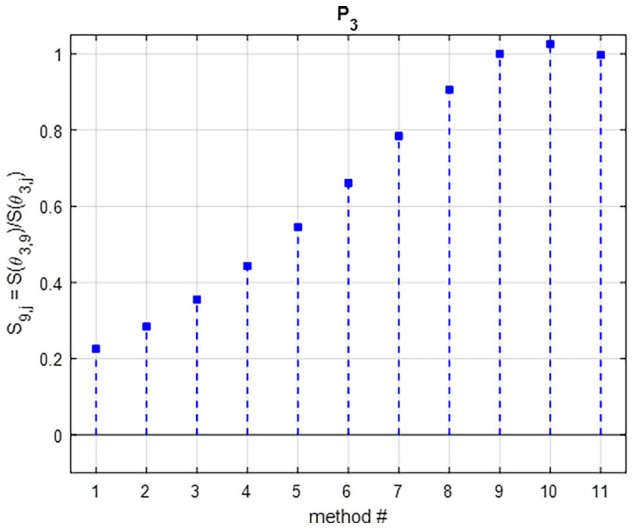

Fig. 32 Relative performance values calculated using techniques #1-11 with respect to the one calculated using technique #9 for the process P_3

around $x_2 = 65\%$ across various fractional dynamics within the order range $0.50 \leq \alpha \leq 1.00$.

The method proposed in this paper introduces several novel aspects compared to the authors' previous work. More specifically:

1. The relationship between model accuracy and the central point's location has been established. This behavior has been generalized for various fractional-order dynamics.
2. A selection criterion for x_2 has been established to minimize the model's accuracy.

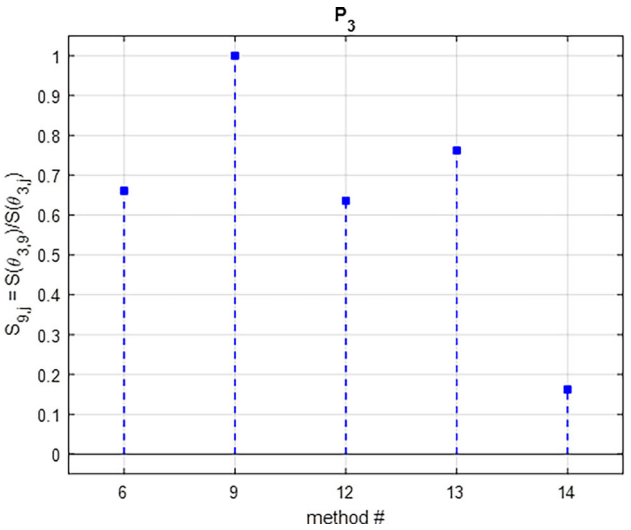

Fig. 33 Relative performance values calculated using techniques #6 and #12-14 with respect to the one calculated using technique #9 for the process P_3

3. Compared to the method proposed in [33], improvements are primarily based on more accurate estimations of the α parameter.
4. The problem and methodology of the experimental procedure used are clearly defined in Sect. 4.
5. These contributions have been validated through simulation, using several examples commonly found in the literature. In particular, Example 1 in Sect. 5.1 extensively evaluates 99 fractional-order processes with orders in the range $\alpha \in [0.6, \ldots, 1.0]$.

This section demonstrates a significant improvement in accuracy across multiple fractional-order process models when the central value is adjusted to $x_2 = 65\%$. This adjustment enhances the effectiveness of the identification technique and retains its essential characteristics:

1. This analytical method significantly simplifies hardware implementation, as discussed further in Sect. 6.
2. The method's simplicity stems from the straightforward physical interpretation and ease of application of the three-point identification approach. Simplicity is maintained since the value of the central point is fixed at $x_2 = 65\%$ and the symmetry of the remaining points, x_1 and x_3, is also held. Furthermore, the recommendations provided in [33] for the selection of the x-value remain valid for this procedure.
3. This identification method is highly effective and improves the model's accuracy. The reduction of the performance index S when moving central point x_2 to 65% compared to $x_2 = 50\%$ has been quantified. More specifically, the reduction in S is 30% for $P_{1,5}$, 36% for P_2, and 34% for

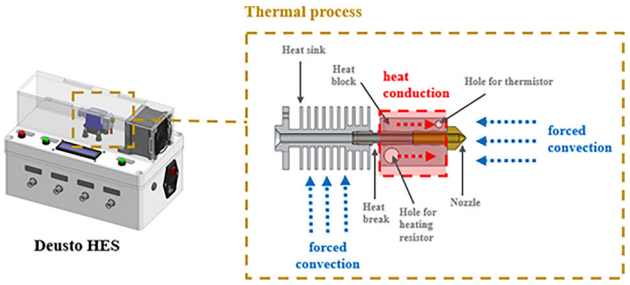

Fig. 34 Scheme of Deusto HES equipment, including a detailed picture of the thermodynamic phenomena in the extruder head

P_3. The proposed identification method demonstrates a significant improvement in accuracy compared to well-known identification methods, including those based on optimization techniques.

Additionally, while this paper does not address measurement noise and model uncertainty, these aspects have been thoroughly discussed in [32].

6 Experimental results

The objectives to be fulfilled in this section are the following: First, to confirm that the proposed identification procedure can be applied to an experimental prototype; and second, to understand the practical aspects of applying the proposed algorithm on industrial hardware. This section is divided as follows: first, a brief overview of the temperature-based experimental setup is presented. Then, the proposed identification technique for (x-x_2-$(100-x)\%$) is implemented on a microprocessor hardware. The procedure is then applied to an experimental setup, thus verifying the applicability of the FFOPDT model identification technique to industrial equipment. Finally, we address practical considerations related to the hardware implementation, more specifically on a microprocessor-based platform, and conclude with some final remarks.

6.1 Thermal-based experimental setup

This section utilizes an experimental setup based on a hardware-in-the-loop system. Figure 34 illustrates the Deusto Heater Experimental Setup (HES), which is the equipment being considered. The thermal process occurs at the top of the prototype, where an air fan and the extruder head of a 3D printer are housed within a methacrylate duct. This figure also highlights the thermodynamic phenomena occurring in the extrusion head. Although the prototype supports several configurations [42], the one used in this study maintains a constant air fan speed, with the heating resistor functioning as the actuator. For a more comprehensive description of this equipment, see [41, 42].

6.2 FFOPDT model estimation

To implement the identification procedure and verify our results, we utilized the hardware architecture described in [43] along with the experimental prototype.

The hardware consists of an NI myRIO-1900 device, selecting its onboard microprocessor to implement the FFOPDT model identification method, with LabVIEW used as the programming environment. Figure 35 illustrates the complete layout of the experimental setup, including the microprocessor-based device employed as hardware for the practical implementation of the identification algorithms discussed in this paper.

The identification technique described in Algorithm 1, based on the representative points (x-x_2-$(100-x)\%$), was implemented using LabVIEW on the microprocessor device. The required process data to determine model parameters θ_P are the process output variation Δy, the input signal variation Δu, and the times taken to achieve $x\%$ (t_x), $x_2\%$ (t_{x2}), and $(100-x)\%$ (t_{100-x}) of the total response interval, as indicated in Algorithm 1.

Algorithm 1 Identification technique with symmetrical points (x-x_2-$(100-x)\%$)

Require: $\{t_x, t_{x2}, t_{100-x}, \Delta y, \Delta x\}$
Ensure: $\theta_P = \{K, T, L, \alpha\}$
1: Determine the process gain: $K = \frac{\Delta y}{\Delta u}$.
2: Extract the times t_x, t_{x2}, and t_{100-x} from the process reaction curve.
3: Determine the ratio index: $\Delta = \frac{t_{100-x}-t_x}{t_{x2}-t_x}$.
4: Compute $\alpha = f_1(\Delta)$.
5: Use the rational expressions to find $f_2(\alpha)$ and $f_3(\alpha)$.
6: Calculate $T = f_2(\alpha) \cdot (t_{100-x} - t_x)^{\alpha}$.
7: Derive $L = \max\left[t_{100-x} - f_3(\alpha) \cdot T^{\frac{1}{\alpha}}, 0\right]$.
8: Fractional model parameters: $\theta_P = \{K, T, L, \alpha\}$

Figures 36 and 37 present the process data used to identify the reduced-order model at a specific operating point. Initially, the command signal u_F is held constant at 10%, while a step input with a magnitude of $\Delta u_H = 30\%$ is applied to the heating element (see Fig. 36). At this operating point, the temperature $T_m(t)$ exhibits a change of $\Delta T_m = 42^oC$, increasing from 60.5^oC to 102.5^oC (see Fig. 37). Note that the output signal is effectively filtered using a first-order low-pass filter, and the sample time for this experiment was $T_S = 100$ ms.

These figures provide the signal data used to determine the process parameters listed in Table 18. Table 19 summarizes the FFOPDT model parameters derived with the technique detailed in [32] for the points (10–50–90%) and (10–65–90%). Then, Figs. 38 and 39 illustrate the process

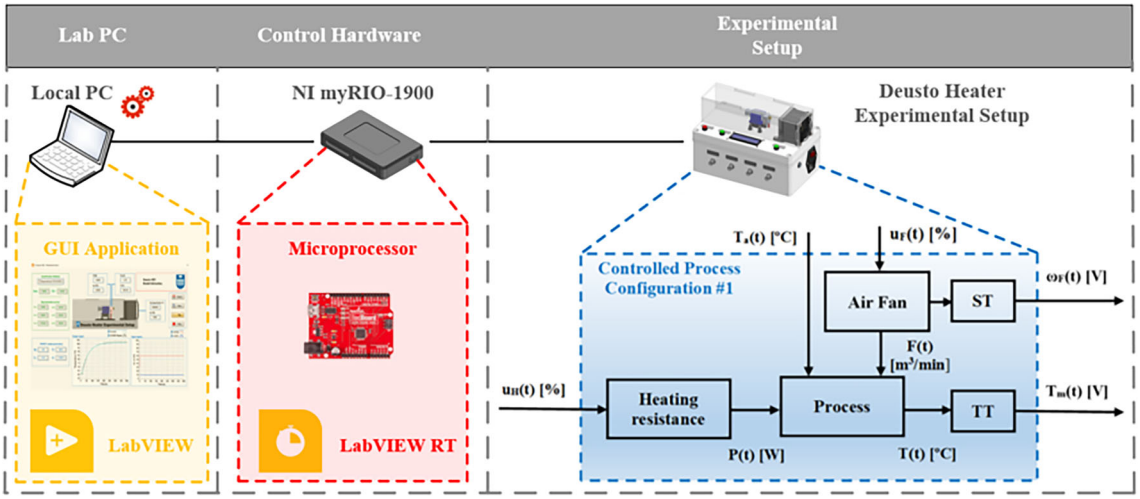

Fig. 35 Overview of the experimental setup for implementing model identification algorithms on a microprocessor-based device. The figure also contains a block diagram with the configuration of the thermal process

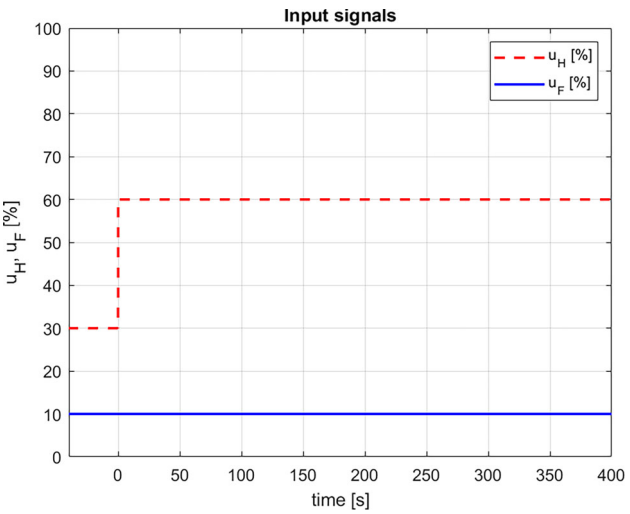

Fig. 36 Input signal $u_H(t)$, in the form of a step with $\Delta u_H = 30\%$, and the command signal $u_F(t) = 10\%$ applied to the thermal process in the experimental prototype

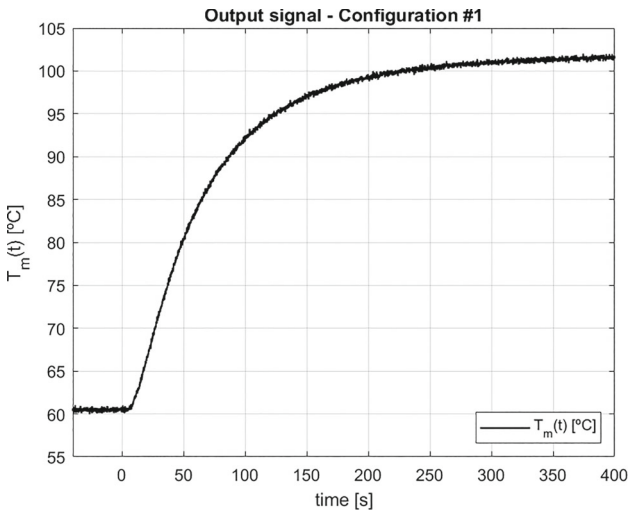

Fig. 37 Output signal $T_m(t)$ $[^oC]$ of the thermal process in the experimental prototype

Table 18 Process information required for the thermal process

Method #6		Method #9
	$\Delta y = \Delta T_m = 42^oC$	
	$\Delta u = \Delta u_H = 30\%$	
	$t_{10} = 16.80$ s	
$t_{50} = 53.30$ s		$t_{65} = 76.10$ s
	$t_{90} = 174.50$ s	

Table 19 FFOPDT model parameters identified employing the developed technique with sets of points (10–50–90%) and (10–65–90%) for the thermal process

Method #6	Method #9
$K_{4,6} = 1.40^oC/\%$	$K_{4,9} = 1.40^oC/\%$
$T_{4,6} = 49.83$ s	$T_{4,9} = 46.62$ s
$L_{4,6} = 11.08$ s	$L_{4,9} = 11.49$ s
$\alpha_{4,6} = 0.9468$	$\alpha_{4,9} = 0.9373$

response and the step responses of fractional-order models whose parameters are detailed in Table 19.

The models obtained using methods #1-11 are presented, with Table 20 displaying the values of $S(\theta_{4,j})$ for each identification technique ($j = 1, \ldots, 11$) applied to the thermal process. Figure 40 visually illustrates the data summarized in Table 20. The behavior observed in the temperature-based process mirrors that of the examples in Sect. 5, exhibiting a minimum value in $S(\theta_{4,j})$ for $x_2 > 50\%$. Specifically, the

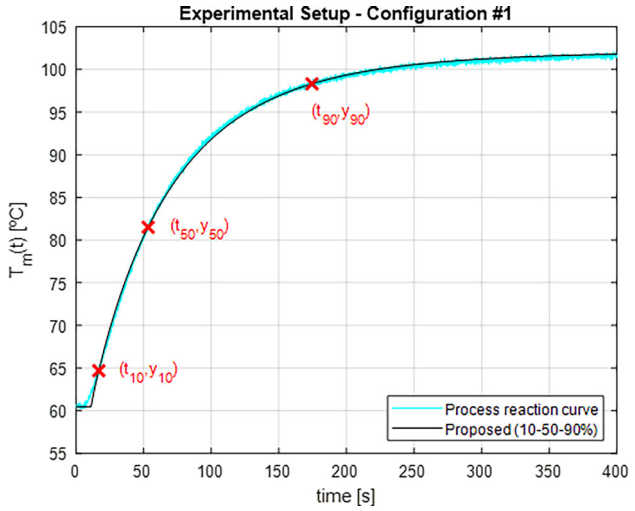

Fig. 38 Step response of the FFOPDT model identified by employing the developed technique for (10–50–90%)

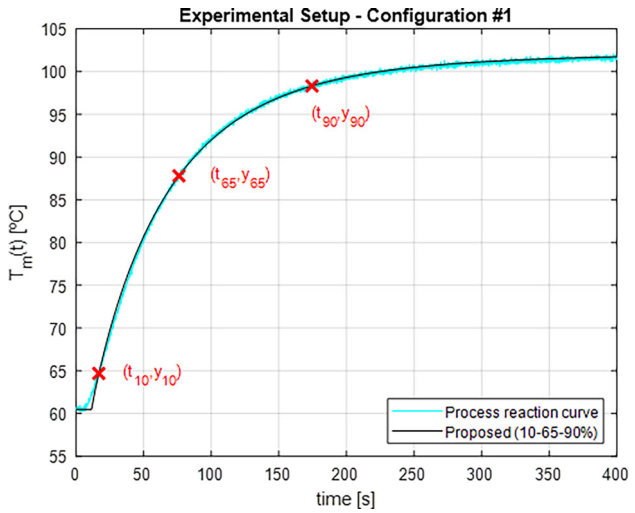

Fig. 39 Step response of the FFOPDT model identified by employing the developed technique for (10–65–90%)

Table 20 Performance index $S(\theta_{4,j})$ computed for the FFOPDT models determined employing the identification techniques considered with $j = 1, \ldots, 11$ for the thermal process

j	Method	Model	x_2 (%)	Set of points	$S(\theta_{4,j})$
1	#1	FFOPDT	25	(10–25–90%)	3.12×10^{-4}
2	#2	FFOPDT	30	(10–30–90%)	2.20×10^{-4}
3	#3	FFOPDT	35	(10–35–90%)	1.62×10^{-4}
4	#4	FFOPDT	40	(10–40–90%)	1.15×10^{-4}
5	#5	FFOPDT	45	(10–45–90%)	9.02×10^{-5}
6	#6	FFOPDT	50	(10–50–90%)	7.34×10^{-5}
7	#7	FFOPDT	55	(10–55–90%)	6.68×10^{-5}
8	#8	FFOPDT	60	(10–60–90%)	6.50×10^{-5}
9	#9	FFOPDT	65	(10–65–90%)	6.70×10^{-5}
10	#10	FFOPDT	70	(10–70–90%)	7.28×10^{-5}
11	#11	FFOPDT	75	(10–75–90%)	8.01×10^{-5}
			$N_S = 4001$		

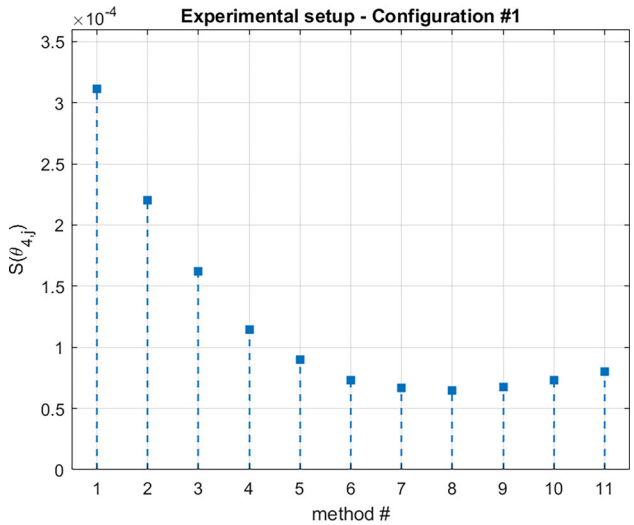

Fig. 40 Values of $S(\theta_{4,j})$ calculated using methods #1-11 for the thermal process

minimum occurs at $x_2 = 60\%$ ($j = 8$), although the difference from $x_2 = 65\%$ ($j = 9$) is negligible. Performance indices increase slightly for values of x_2 above 60%, as discussed in Sect. 5. In this case, using $x_2 = 65\%$ instead of $x_2 = 50\%$ results in an 8.7% reduction in S.

The proposed approach is compared with other identification techniques for FFOPDT models that are based on the reaction curve. Specifically, the symmetrical approach proposed for $x_2 = 65\%$ is compared with the symmetrical and asymmetrical methods presented in [32], corresponding to the points (10–50–90%) and (20–60–95%), respectively, as well as with the method proposed by Nie in [44]. Additionally, comparisons are included with the optimal methods for FOPDT and DPPDT models.

Table 21 presents the parameters of the FFOPDT model for the thermal process at the considered operating point, obtained using the previously selected techniques. The MSE values calculated for these models are shown in Table 22. Based on this data, it can be observed that the proposed method delivers satisfactory results compared to other techniques for FFOPDT models based on the process reaction curve. Specifically, the S values obtained with the proposed symmetrical method for $x_2 = 65\%$ are 8.7%, 43.2%, and 32.0% lower than those obtained with the symmetrical, asymmetrical, and Nie's methods, respectively.

Furthermore, any of the FFOPDT model identification methods significantly outperforms the MSE optimization-based methods for FOPDT and DPPDT models, confirming

Table 21 FFOPDT model parameters identified using different identification techniques for the thermal process

Method	Model	Set of points	K (°C/%)	T (s)	L (s)	α
Proposed	FFOPDT	(10–65–90%)	1.40	46.62	11.49	0.9373
Symmetrical [32]	FFOPDT	(10–50–90%)	1.40	49.83	11.08	0.9468
Asymmetrical [32]	FFOPDT	(20–60–95%)	1.40	47.28	11.05	0.9333
Nie [44]	FFOPDT	(20–60–95%)	1.40	43.39	13.62	0.9279
Optimal FOPDT	FOPDT	–	1.40	69.10	7.55	–
Optimal DPPDT	DPPDT	–	1.40	32.43	0.00	–

the superiority of fractional-order models over integer-order models for modeling purposes.

Therefore, it can be concluded that the proposed approach achieves more accurate estimation of FFOPDT models compared to other well-established methods, while maintaining the simplicity of the procedure.

Figure 41 shows the front panel of the interface implemented using LabVIEW for FFOPDT model identification. This figure highlights the various features available in the LabVIEW-based application:

1. Selection of the symmetrical method, including $x\%$ and $x_2\%$ for $(x\text{-}x_2\text{-}(100-x)\%)$.
2. Obtaining process information $\{\Delta y, \Delta u, t_x, t_{x2}, t_{100-x}\}$.
3. Estimation of $\theta_P = \{K, T, L, \alpha\}$.
4. Two charts for recording the different variables and responses. One of them shows $u_F(t)$ [%] and $u_H(t)$ [%], while the other one shows $T_m(t)$ [^oC], the reduced-order fractional model step response, and the selected set $(t_x, T_m(t_x))$, $(t_{x2}, T_m(t_{x2}))$, and $(t_{100-x}, T_m(t_{100-x}))$.
5. Determination of S (model performance index).
6. Export the process variables as text- or excel-format.

6.3 Discussion and final remarks

Fractional behavior appears in processes of different natures: physical, electrical, biological, and thermal-based processes, among others [10, 11, 45, 46]. There is a wide variety of natural processes that exhibit fractional behavior. Many of them, with α-values in the range considered in this work, can be typically encountered in many engineering applications. Note that thermal processes are particularly significant in the process industry [12, 13].

Given that this type of behavior is ubiquitous, the availability of this type of identification procedures for fractional reduced-order models such as the one used in this paper is of significant interest in the industrial environment. Furthermore, any accuracy improvement in the identification methods of the identified model is of major relevance.

This section discusses the usefulness and improvement obtained with the considered FFOPDT model identification method by moving the central point x_2 with respect to $x_2 = 50\%$ in an industrial context. The main purpose is to validate the relevance of the identification method and assess the effect of varying x_2's position when when applied to industrial hardware and tested with an experimental prototype.

Without loss of generality, the identification technique presented in this work is implemented on microprocessor-based hardware. However, it is equally adaptable to any technology compatible with the hardware architecture described in [43]. As discussed above, the FFOPDT model identification method is analytical and may be easily implemented on any hardware device.

Concerning the practical aspects of implementing this method on microprocessor hardware, several key considerations emerge in the context of the identification technique explored in this work:

1. The considered identification procedure requires the following process data: $\{\Delta y, \Delta u, t_x, t_{x2}, t_{100-x}\}$.
2. The reaction curve can be stored by using two vectors: one containing the temperature information (T_m) and another with the time information (t). Both vectors are characterized by several points N_S, a sampling period T_S, and a total duration $N_S T_S$.
3. Determining the times t_x, t_{x2}, and t_{100-x} (with $0 < x < 50$ and $x < x_2 < 100 - x$) in terms of software involves traversing the vector T_m to locate the amplitudes corresponding to $x\%$ $(T_m(t_x))$, $x_2\%$ $(T_m(t_{x2}))$, and $(100-x)\%$ $(T_m(t_{100-x}))$, respectively.
4. The FFOPDT model parameters are obtained using $\{\Delta y, \Delta u, t_x, t_{x2}, t_{100-x}\}$ and applying the analytical Equations (25), with $x_1 = x$ and $x_3 = 100 - x$. Additionally, the analytical formulas for f_1, f_2, and f_3 calculated for the points $(x\text{-}x_2\text{-}(100-x)\%)$.
5. Methods for identifying process models that involve selecting specific points from the response curve are generally straightforward to implement. Examples include fractional-order model identification, as described in [33], and integer-order model identification, as outlined in [4].
6. As observed, implementing this identification procedure is straightforward on hardware platforms due to its analytical nature.

Table 22 Performance index $S(\theta_{4,j})$ computed for the FFOPDT models determined employing the reaction curve-based identification techniques, with $j = 1, \ldots, 6$, for the thermal process

j	Method	Model	Set of points	$S(\theta_{4,j})$
1	Proposed	FFOPDT	(10–65–90%)	6.70×10^{-5}
2	Symmetrical [32]	FFOPDT	(10–50–90%)	7.34×10^{-5}
3	Asymmetrical [32]	FFOPDT	(20–60–95%)	1.18×10^{-4}
4	Nie [44]	FFOPDT	(20–60–95%)	9.85×10^{-5}
5	Optimal FOPDT	FOPDT	–	5.80×10^{-4}
6	Optimal DPPDT	DPPDT	–	9.40×10^{-4}
		$N_S = 4001$		

7. Unlike MATLAB, LabVIEW lacks a specific toolkit for fractional systems. Thus, the simulation of the FFOPDT model step response in LabVIEW was implemented by approximating the non-integer differential operators using a discretization of the Grünwald-Letnikov definition for fractional derivatives. However, other approximation methods are also possible.

Some remarks and limitations

This section presents some observations and limitations of the approach proposed in this work, particularly regarding its practical application.

The proposed approach is used for the identification of processes exhibiting fractional behavior, characterized by a monotonic S-shaped response. These types of processes, commonly found in process control [3], can be modeled using an FFOPDT model with a fractional order in the range of $0.50 \leq \alpha \leq 1.00$.

In an industrial environment, it is common for the feedback signal of the controlled process to contain measurement noise. This requires appropriate filtering when the signal is used for model identification and control. Since the filter dynamics will be an integral part of the controlled process to be identified, the proposed identification procedure does not account for the measurement noise [47].

Finally, because the proposed identification method is analytical, it requires low computational effort. This ensures that the characteristics of the hardware used do not limit the effectiveness of the procedure.

Implementing algorithms for identifying fractional models on hardware and applying them to a laboratory prototype has provided valuable insights into practical implementation

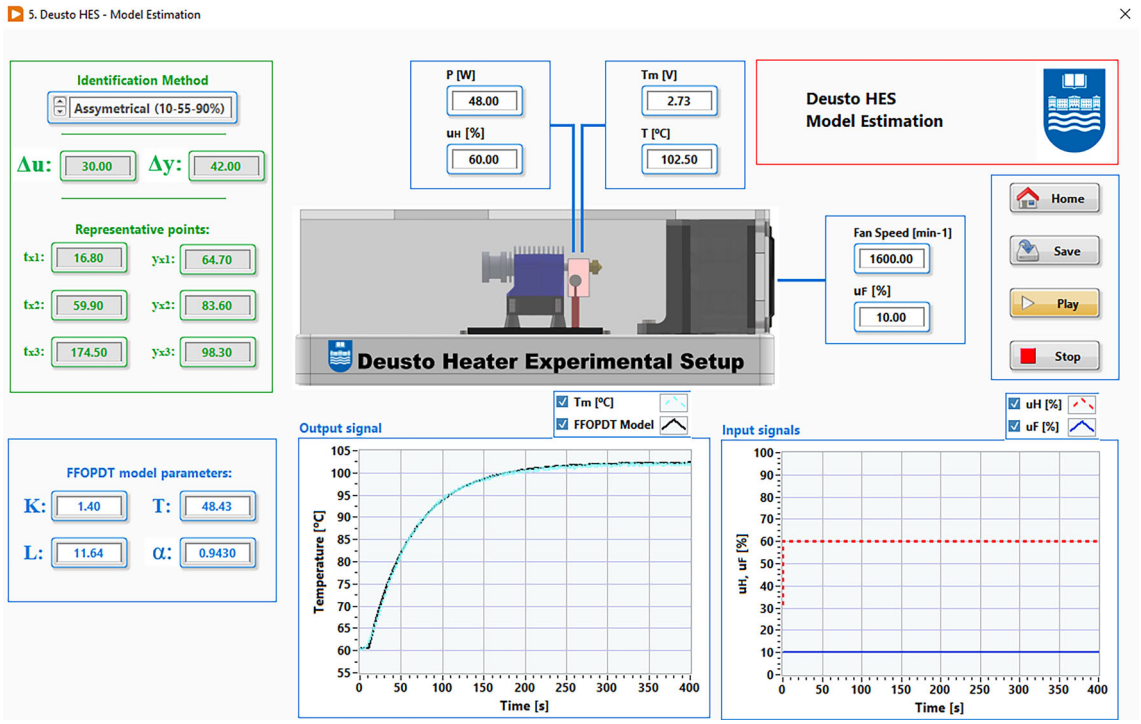

Fig. 41 Graphical user interface of the LabVIEW application to implement model identification algorithms on a microprocessor-based device

challenges. This experience will help demonstrate the benefits of using fractional-order models, recognized in technical literature for their enhanced accuracy in modeling, in industrial applications.

7 Conclusions

This paper introduces an FFOPDT model identification technique that fits three symmetrical points of the process response curve. This technique aims the improvement of the FFOPDT model's accuracy through the adjustment of the position of x_2, while preserving the symmetry of points x_1 and x_3 relative to the middle of the output interval.

This study reveals that the position of x_2 has a substantial effect on the approximate FFOPDT model's accuracy. To confirm these results, an experimental procedure has been designed and implemented. In particular, a more accurate FFOPDT model can be achieved by increasing x_2 to approximately 65%, significantly improving the accuracy within the context of the identification procedure considered here. Additionally, the study provides new insights into selecting x_2, emphasizing that the improvement in model accuracy is primarily due to a more precise estimation of the parameter α.

Various simulation examples were employed to illustrate the effectiveness and practical application of this technique, while also exploring the impact of x_2 on model accuracy. Additionally, a hardware-in-the-loop thermal prototype was employed to validate these findings in the context of microprocessor-based hardware implementation.

For industrial applications, note that this approach is analytical and involves less computational effort than more complex, optimization-based algorithms. In large-scale process industries, which often include many hundreds of control loops, the simplicity of the proposed method makes it particularly valuable for model identification in control applications.

The following lines of future work are suggested in the context of this research:

- Given that the workhorse in the process industry is the programmable logic controller (PLC), these identification procedures must be implemented in a PLC in order for this research to have an impact at the industrial level.
- Hybrid identification methods that combine analytical and optimization-based methods should be explored.

We believe that emphasizing simplicity in identification methods will help connect theoretical studies of fractional modeling with their practical implementation in the industrial sector, thereby promoting their adoption in industry. This expectation serves as a key motivation for our current work.

Appendix A Glossary of acronyms

BIBO bounded-input bounded-output
DPPDT dual-pole plus dead time
FFOPDT fractional first-order plus dead time
FOPDT first-order plus dead time
FOTF fractional-order transfer function
FSOPDT fractional second-order plus dead time
HES heater experimental setup
LabVIEW Laboratory Virtual Instrument Engineering Workbech
MATLAB MATrix LABoratory
MSE mean squared error
PLC programmable logic controller
SOPDT second-order plus dead time

Acknowledgements The authors acknowledge funding support from Basque Government, through the Research Group D4K - Deusto for Knowledge (IT1528) and the BEREZ-IA Elkartek project (KK-2023/00012).

Author Contributions All authors contributed to the study, conception and design. Material preparation, data collection, and analysis were performed by [Juan J. Gude]. The first draft of the manuscript was written by [Juan J. Gude] and all authors commented on previous versions of the manuscript. All authors read and approved the final manuscript. Conceptualization was done by [Juan J. Gude] and [Pablo García Bringas]; [Juan J Gude] was involved in methodology, formal analysis, and investigation; [Juan J. Gude] and [Pablo García Bringas] contributed in writing—original draft preparation and writing—review and editing; [Pablo García Bringas] contributed to funding acquisition; [Pablo García Bringas] helped in resources; supervision was done by [Juan J. Gude] and [Pablo García Bringas].

Funding Open Access funding provided thanks to the CRUE-CSIC agreement with Springer Nature.

Availability of data and materials The data sets used to support the findings of this study are included within the article.

Declarations

Conflict of interest The authors declare no known conflict of interest or personal relationships that could have appeared to influence the work reported in this paper.

References

1. Liu T, Gao F (2011) Industrial process identification and control design: step-test and relay-experiment-based methods. Springer
2. Huang HP, Jeng JC (2005). In: Johnson MA, Moradi MH (eds) Process reaction curve and relay methods identification and PID tuning. Springer, London, pp 297–337
3. Åström KJ, Hägglund T (2006) Advanced PID control. Systems and Automation Society, ISA-The Instrumentation
4. Alfaro V (2006) Low-order models identification from the process reaction curve. Ciencia y Tecnología (Costa Rica) 24(2):197–216
5. Smith CL (1972) Digital computer process control. Intext Educational Publishers
6. Vítečková M, Víteček A, Smutnỳ L (2000) Simple PI and PID controllers tuning for monotone self-regulating plants. IFAC Proc Vol 33(4):259–264
7. Jahanmiri A, Fallahi H (1997) New methods for process identification and design of feedback controller. Chem Eng Res Des 75(5):519–522
8. Mollenkamp RA (1984) Introduction to automatic process control. ISA International Society for Measurement and Control
9. Rangaiah GP, Krishnaswamy PR (1994) Estimating second-order plus dead time model parameters. Ind Eng Chem Res 33(7):1867–1871
10. Dzieliński A, Sierociuk D, Sarwas G (2010) Some applications of fractional order calculus. Bull Pol Acad Sci Techn Sci 4
11. Tenreiro Machado J, Silva MF, Barbosa RS, Jesus IS, Reis CM, Marcos MG et al (2010) Some applications of fractional calculus in engineering. Math Probl Eng 2010(1):639801
12. Žecová M, Terpák J (2015) Heat conduction modeling by using fractional-order derivatives. Appl Math Comput 257:365–373
13. Yuan J, Ding Y, Fei S, Chen Y (2022) Identification and parameter sensitivity analyses of time-delay with single-fractional-pole systems under actuator rate limit effect. Mech Syst Signal Process 163:108111
14. Podlubny I (1998) Fractional differential equations: an introduction to fractional derivatives, fractional differential equations, to methods of their solution and some of their applications. Elsevier
15. Monje CA, Chen Y, Vinagre BM, Xue D, Feliu-Batlle V (2010) Fractional-order systems and controls: fundamentals and applications. Springer
16. Tepljakov A (2017) Fractional-order modeling and control of dynamic systems. Springer
17. Malti R, Victor S, Oustaloup A (2008) Advances in system identification using fractional models. J Comput Nonlinear Dyn 3(2):021401
18. Guevara E, Meneses H, Arrieta O, Vilanova R, Visioli A, Padula F (2015) Fractional order model identification: computational optimization. In: 2015 IEEE 20th conference on emerging technologies & factory automation (ETFA). IEEE, pp 1–4
19. Malek H, Luo Y, Chen Y (2013) Identification and tuning fractional order proportional integral controllers for time delayed systems with a fractional pole. Mechatronics 23(7):746–754
20. Alagoz BB, Tepljakov A, Ates A, Petlenkov E, Yeroglu C (2019) Time-domain identification of one noninteger order plus time delay models from step response measurements. Int J Model Simul Sci Comput 10(01):1941011
21. Narang A, Shah SL, Chen T (2011) Continuous-time model identification of fractional-order models with time delays. IET Control Theory Appl 5(7):900–912
22. Ahmed S (2010) Process identification using nonideal step inputs. IFAC Proc Vol 43(5):367–372
23. Ahmed S (2016) Identification from step response-The integral equation approach. Can J Chem Eng 94(12):2243–2256
24. Fahim SM, Ahmed S, Imtiaz SA (2018) Fractional order model identification using the sinusoidal input. ISA Trans 83:35–41
25. Tavakoli-Kakhki M, Haeri M, Tavazoei MS (2010) Simple fractional order model structures and their applications in control system design. Eur J Control 16(6):680–694
26. Tavakoli-Kakhki M, Saleh TM (2014) Estimation of the order and parameters of a fractional order model from a noisy step response data. J Dyn Syst Meas Contr 136(3):031020
27. Tavakoli-Kakhki M, Tavazoei MS, Mesbahi A (2013) Parameter and order estimation from noisy step response data. IFAC Proc Vol 46(1):492–497
28. Gude JJ, Kahoraho E (2009) New tuning rules for PI and fractional PI controllers. IFAC Pro Vol 42(11):768–773
29. Gude JJ, Kahoraho E (2009) Simple tuning rules for fractional PI controllers. In: 2009 IEEE conference on emerging technologies & factory automation. IEEE, pp 1–8
30. Meneses H, Arrieta O, Padula F, Visioli A, Vilanova R (2022) Fopi/fopid tuning rule based on a fractional order model for the process. Fractal Fractional 6(9):478
31. Gude JJ, Di Teodoro A, Herrera M, Rincón L, Camacho O et al (2024) Sliding mode control design using a generalized reduced-order fractional model for chemical processes. Results Eng 24:103032
32. Gude JJ, García Bringas P (2022) Proposal of a general identification method for fractional-order processes based on the process reaction curve. Fractal Fractional 6(9):526
33. Gude JJ, García Bringas P (2022) Influence of the selection of reaction curve's representative points on the accuracy of the identified fractional-order model. J Math 2022(1):7185131
34. Gude JJ, Di Teodoro A, Camacho O, García Bringas P (2023) A new fractional reduced-order model-inspired system identification method for dynamical systems. IEEE Access
35. Kilbas A (2006) Theory and applications of fractional differential equations. North-Holland Math Stud 204
36. Gorenflo R, Kilbas AA, Mainardi F, Rogosin SV, et al (2020) Mittag-Leffler functions, related topics and applications. Springer
37. Rogosin S (2015) The role of the Mittag-Leffler function in fractional modeling. Mathematics 3(2):368–381
38. Smith CA, Corripio AB (2005) Principles and practices of automatic process control. Wiley
39. Åström KJ, Hägglund T (2004) Revisiting the Ziegler-Nichols step response method for PID control. J Process Control 14(6):635–650
40. Xue D (2017) Fractional-order control systems: fundamentals and numerical implementations. vol. 1. Walter de Gruyter GmbH & Co KG
41. Gude JJ (2023) Contributions to fractional-order modelling and control of dynamic systems: a theoretical and practical approach. Universidad de Deusto
42. Gude JJ, García Bringas P (2024) Proposal of a control hardware architecture for implementation of fractional-order controllers. In: Awrejcewicz J (ed) Perspectives in Dynamical Systems II—Numerical and Analytical Approaches. Springer International Publishing, Cham, pp 229–262
43. Gude JJ, García Bringas P (2022) A novel control hardware architecture for implementation of fractional-order identification and control algorithms applied to a temperature prototype. Mathematics 11(1):143
44. Nie Z, Wang Q, Liu R, Lan Y (2016) Identification and PID control for a class of delay fractional-order systems. IEEE/CAA J Automatica Sinica 3(4):463–476
45. Agrawal H, Singh A, Sharma H, Purohi S, et al (2024) Age-based investigation of COVID-19 prevalence in Ethiopia using mathematical modelling. South East Asian J Math Math Sci 20(1)
46. Meena M, Purohit M et al (2024) Mathematical analysis using fractional operator to study the dynamics of dengue fever. Phys Scr 99(9):095206

47. Romero Segovia V, Hägglund T, Åström KJ (2014) Measurement noise filtering for PID controllers. J Process Control 24(4):299–313